EXTENDED KALMAN FILTER ESTIMATION BASED CONTROL OF DOUBLE TWIN ROTOR AERODYNAMIC SYSTEM

A THESIS SUBMITTED TO

GRADUATE SCHOOL OF NATURAL AND APPLIED SCIENCES

OF

KOCAELI UNIVERSITY

BY

FAZAL E NASIR

IN PARTIAL FULFILLMENT OF THE REQUIREMENTS

FOR

THE DEGREE OF MASTER OF SCIENCE

IN

MECHATRONICS ENGINEERING

KOCAELI 2019

EXTENDED KALMAN FILTER ESTIMATION BASED CONTROL

OF DOUBLE TWIN ROTOR AERODYNAMIC SYSTEM
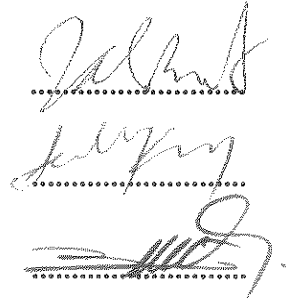
A THESIS SUBMITTED TO

GRADUATE SCHOOL OF NATURAL AND APPLIED SCIENCES

OF

KOCAELİ UNIVERSITY

BY

FAZAL E NASIR

IN PARTIAL FULFILLMENT OF THE REQUIREMENTS
FOR
THE DEGREE OF MASTER OF SCIENCE
IN
MECHATRONICS ENGINEERING

Prof.Dr. Zafer BİNGÜL
Supervisor,   Kocaeli University
Assist.Prof.Dr. Selçuk KİZİR
Jury member,   Kocaeli University
Assist.Prof.Dr. Metin TOZ
Jury member,   Düzce University

Thesis Defense Date: 08.07.2019

ACKNOWLEDGMENT

CONTENTS

LIST OF FIGURES

LIST OF TABLES

LIST OF SYMBOLS AND ABBREVIATIONS

θ	: Pitch angle, (degrees)
ψ	: Yaw angle, (degrees)
φ	: Roll angle, (degrees)
ω_{mu}	: Angular velocity of up motor of pitch rotor, (rads^{-1})
ω_{md}	: Angular velocity of down motor of pitch rotor, (rads^{-1})
ω_{ml}	: Angular velocity of left motor of yaw rotor, (rads^{-1})
ω_{mr}	: Angular velocity of right motor of yaw rotor, (rads^{-1})
m_{ts}	: Tail motor shield mass, (kg)
m_{mm}	: Main motor mass, (kg)
m_{ms}	: Main motor shield mass, (kg)
m_{tb}	: Tail beam mass, (kg)
m_{mb}	: Main beam mass, (kg)
m_{cb}	: Counter weight beam mass, (kg)
m_{cm}	: Counter weight mass, (kg)
l_t	: Tail beam length, (m)
l_m	: Main beam length, (m)
l_c	: Counter beam length, (m)
U_ψ	: Yaw motors total force, (N)
U_θ	: Pitch motors total force, (N)
J_θ	: Moment of inertia about pitch axis, (kgm^2)
J_ψ	: Moment of inertia about yaw axis, (kgm^2)
E_{mtb}	: Moment due to weight of tail beam about pitch axis, (Nm)
E_T	: Moment due to pitch motors thrust about pitch axis, (Nm)
E_{cb}	: Moment due to weight of counter beam about pitch axis, (Nm)
E_{cg}	: Moment due to centrifugal force about pitch axis, (Nm)
E_f	: Moment due to friction force about pitch axis, (Nm)
A,B,C,D,E,F,G	: Mass constants, (kg)
k_p	: Friction constant of pitch joint
k_y	: Friction constant of yaw joint
A_T	: Moment due to yaw motors thrust about yaw axis, (Nm)
A_f	: Moment due to friction force about yaw axis, (Nm)
χ_r	: Thrust force of right motor, (N)
χ_l	: Thrust force of left motor, (N)
T	: Thrust force by propeller, (N)
Q	: Torque due to propeller, (Nm)
ω	: Angular velocity of propeller, (rads^{-1})
R	: Radius of propeller, (m)
C_T	: Propeller thrust coefficient
C_Q	: Propeller torque coefficient
ρ	: Density of air, (kgm^{-3})
A	: Area of propeller disc, (m^2)

$P_{electrical}$	: Electrical power of motor, (W)
$P_{mechanical}$	: Mechanical power of motor, (W)
$\eta_{motor+ESC}$	: Efficiency of motor
M_g	: Moment due to gravity, (Nm)
T_u	: Up motor throttle, (duty cycle)
T_d	: Down motor throttle, (duty cycle)
y_i	: IMU sensors calibrated output
M_i	: IMU sensor sensitivity parameter
S_i	: IMU sensor scaling factor
b_i	: IMU sensor bias value
v_i	: IMU sensor white noise value
θ_a	: Pitch angle from accelerometer gravity vector, (degrees)
φ_a	: Roll angle form accelerometer gravity vector, (degrees)
θ_g	: Integration of Euler's pitch rate, (degrees)
φ_g	: Integration of Euler's roll rate, (degrees)
p,q r	: Gyroscope sensor angular rate output, $(degs^{-1})$
w_k, v_k	: Process and measurement white noise
P_k	: Covariance error, (degrees)
K_k	: Kalman gain
X_s	: Actual signal, (W)
N_s	: Noisy signal, (W)
u_c	: Controller signal, (duty cycle)
θ_r	: Reference pitch angle trajectory, (degrees)
θ_P	: Current pitch angle, (degrees)
θ_y	: Current yaw angle, (degrees)
K_P	: Controller position gain
K_V	: Controller velocity gain
K_A	: Controller acceleration gain
Π_D	: Actual control signal for up motor, (duty cycle)
Γ	: Gravity compensation function, (duty cycle)
u_{uac}	: Up active controller signal, (duty cycle)
u_{urc}	: Up reactive controller signal, (duty cycle)

Abbreviations

DOF	: Degree Of Freedom
IMU	: Inertial Measurement Unit
EKF	: Extended Kalman Filter
PID	: Proportional Integrator Derivative
UAVs	: Unmanned Aerial Vehicles
MEMS	: Micro Electro Mechanical System
UKF	: Unscented Kalman Filter
PI	: Proportional Integrator
PC	: Personal Computer
DC	: Direct Current
LQ	: Linear Quadratic

LQR	: Linear Quadratic Regulator
LQG	: Linear Quadratic Gaussian
AUV	:Autonomous Underwater Vehicle
PWMs	: Pulse Width Modulations
DTRAS	: Double Twin Rotor Aerodynamic System
ESC	: Electronic Speed Controller
AHRS	: Attitude and Heading Reference System
SNR	: Signal to Noise Ratio
PCB	: Printed Circuit Board
ISE	: Integrated Square Error
CFSF	: Cascaded Full-State Feedback

ÇİFT İKİLİ ROTOR AERODİNAMİK SİSTEMİN EXTENDED KALMAN FİLTRESİ TABANLI KONTROLÜ

ÖZET

Bu tezde geleneksel tek pervaneli helikopter sistemine kıyasla daha hızlı dinamik tepkiler elde ederek performansın arttırılması için tasarlanmış yeni bir 2DOF Aerodinamik Sistemin kontrol tasarım stratejisi ve davranış tahmini ele alınmıştır. Önerilen tasarımda her serbestlik derecesini kontrol etmek için iki eyleyici kullanılmakta böylece tahrik ünitesi tepki olarak daha çevik hale getirilmektedir. Bu tez, temel olarak iki alana odaklanmaktadır: 2DOF Aerodinamik Sistemin davranış bilgilerini tahmin etmek için genişletilmiş Kalman filtresinin uygulanması ve kontrol stratejilerinin uygulanması ve karşılaştırılması.

Bu tezin ana katkıları, fazla tahrikli 2DOF Aerodinamik Sisteminin matematiksel modelinin geliştirilmesi, oryantasyon tahmini ve saha hareketi için yerçekimi dengeleme stratejisinin geliştirilmesidir.

2DOF Aerodinamik Sistemin üç ana bölümünün matematiksel modellenmesi geliştirilmiştir. İlk olarak, sistem gövdesi çerçevesi, motorlar ve motorları tutmak için gerekli bileşenlerden oluşan dönel gövdeler için Newton ikinci yasalarını kullanarak moment denkleminin geliştirilmesi gerçekleştirilmiştir. Bu moment denklemlerini kullanarak, önerilen sistemin dinamikleri Simulink modelinde analiz edilmiştir. İkincisi, itme kuvveti ve tork üretimi için statik deneyler, itme kuvveti ve tork denklemlerinin yaklaşık parametrelerinin tanımlanması ve ayrıca itme sisteminin verimliliğinin analiz edilmesi için yapılmıştır. Üçüncüsü, motorun dinamikleri, bir dizi çeşitli giriş sinyalinin verildiği ve uygun bir transfer fonksiyonunun yaklaştığı bir dizi deney yapılarak tanımlanmıştır.

EKF, teklif edilen sistemin belirsiz durumlarını, yerleşik düşük maliyetli IMU sensöründen gelen gürültülü ölçümlerden tahmin etmek için uygulanır. Bu tahmin edilen durumlar daha sonra arzu tutumunu sürdürmek için kontrol algoritmasında geri bildirim bilgisi olarak kullanılır.

Yerçekimi dengelemesi, yerçekimi kuvveti tarafından oluşturulan torku dengelemek için, perde dinamik kontrol cihazına eklenir. Bu kompanzasyon modeli, perde dinamik modelinin evrilmiş modelinin bulunmasıyla geliştirilmiştir. Elde edilen transfer fonksiyonu, yerçekimi nedeniyle değişen bozulma torkunu dengelemektedir.

Kontrol sisteminin tasarımında yer alan iki ana bölüm, kontrol tahsis algoritması ve kontrol yasasıdır. Kontrol tahsis metodu kontrol sinyallerinin karşılık gelen motor setine programlanmasını içerir. Tasarım tahsisi, gerekli motor sinyallerini almak için durum geri besleme değerlerini yaklaşık kazanç matrisiyle kullanır. Kontrol kanunu tasarlanırken, üç kontrol stratejisi: Tam Durumlu Basamaklı denetleyici, PID denetleyici ve son olarak Bulanık Mantık denetleyici tasarlanmış ve karşılaştırma yapılmıştır.

Anahtar Kelimeler: Aerodinamik Sistem, Basamaklı Kontrol, Bulanık Mantık Kontrolü, Genişletilmiş Kalman Filtresi, IMU.

EXTENDED KALMAN FILTER ESTIMATION BASED CONTROL OF DOUBLE TWIN ROTOR AERODYNAMIC SYSTEM

ABSTRACT

This thesis reports the control strategies and attitude estimation of a novel 2DOF Aerodynamic System, designed for increase in performance by achieving fast dynamic responses compare to the conventional double propeller helicopter system. The proposed design is an overactuted system uses two actuators for controlling each DOF, thus make the propulsion unit more agile in response. This thesis focuses mainly on two areas, the application of extended Kalman filter for states estimation and comparison of control strategies.

The major contributions of this thesis are the development of mathematical model of overactuated 2DOF Aerodynamic System, orientation estimation and developing the gravity compensation strategy for the pitch motion.

The mathematical modeling of three main parts of 2DOF Aerodynamic System are developed. First, developing of moment equation using Newton second laws for rotational bodies that consists of system body frame, motors and necessary components for holding motors. Using these moment equations, the dynamics of the DTRAS system are analyzed in Simulink model. Second, static thrust and torque analysis are carried out for approximating parameters of thrust and torque equations and testing the efficiency of the propulsion system. Third, the dynamics of motor are identified by carrying a series of experiments in which a set of various input signals are given and a fitted transfer function is approximated.

EKF is implemented for estimating the uncertain states of the proposed system from the noisy measurements from the on-board low cost IMU sensor. These estimated states are then used as states feedback information in the control algorithm for sustaining the desire attitude.

The gravity compensation is added to the pitch dynamic controller to compensate for the torque generated by the gravity force. This compensation model is developed by finding the inversion model of the pitch dynamic model. The resultant transfer function compensates the varying disturbance torque due to gravity.

Two main part involve in designing the control system, are the control allocation algorithm and control law. The control allocation method involves the scheduling the control signals to the corresponding set of motors. The design allocator uses the state feedback values with an approximated gain matrix to get the required motors signals. In designing the control law, three control strategies i-e Cascaded Full-State Feedback controller, PID controller and finally Fuzzy Logic controllers are designed and performance comparison is made.

Keywords: Aerodynamic System, Cascaded Control, Extended Kalman Filter, Fuzzy Logic Control, IMU.

INTRODUCTION

The flying principles and constructing design of helicopter and aircraft has been the great interest of the man. Helicopters whether manual or autonomous are used in various applications, from security and military to sport events and leisure activities. But the primary purpose involves investigation of hazardous places like battleship, forest fires, nuclear/chemical leakage areas etc. Governments use UAVs for power and pipeline security, custom/border patrol, rescue operation and social event observations. Considering these applications, the market is growing and new ways to use the technology are discovered at a fast pace. All fields concerning helicopters or UAVs enforce a need of security. The vehicles must be able to operate in dangerous areas, which might lead to malfunctioning sensor equipment, and they must have a reliable way of determining how they are positioned and oriented in the world. Without this reliability, the use of UAVs would be rare.

With the recent technological advancement of computers and the development of modern control theory, automatic control systems are a major factor in the development of almost every new flying vehicle. Therefore, researchers, in aviation industries are focusing to improve the dynamic controls of helicopter system that are nonlinear in nature along with its navigational uncertainties. The advancement of electromechanical system (MEMS) technology made it easy to replace the heavy big and expensive components with small and more precise components. However, these advancements have its limitations and drawbacks that need to deal with especially when the system has uncertainties and noisy measurements. Navigation and attitude estimation is a well-researched and is covered thoroughly in literature, which allows several methods to be chosen from. To estimate the attitude in a controlled environment is a task that can be solved in numerous ways. One such powerful tool in estimation theory is the Kalman Filter.

However, a traditional Kalman Filter cannot be used for a highly non-linear system like a typical flight models. Therefore, an algorithm needed to estimate the parameters

of nonlinear system equations like helicopter system. According to Crassidis et al. [2007] the oldest and most common approach which was first used in the Apollo project is the Extended Kalman filter (EKF) which handles the non-linearities by linearization at the current state estimate, but there are a multitude of other filters which can be applied. Another common approach is the Unscented Kalman filter (UKF) which, however, concluded that the EKF is preferred in most situations due to the flexibility of the approach. The ukf handles severe non-linearities better and does not need a good a priori state estimate. However, the UKF is less intuitive and computationally heavier and since the computational power is limited during this project the EKF is the chosen method. Other methods include Error-State Kalman and Particle filters but these are not investigated further in this thesis.

This research work cover two main goals, attitude states estimation and attitude states control of 2DOF laboratory helicopter system. In first, an extended Kalman Filter is design for attitude states estimation of the helicopter system by using inertial sensors and encoder sensors. In second, control strategies of cascaded PID control, PI cascaded control and Fuzzy logic control had been implemented.

An overactuated system is defined as one that have more actuators then number of degree of freedom that need to be control. In other words, an overactuated system is one that have more control inputs then the variables need to be controlled.

In engineering application, the overactuated systems appear for various reasons. For example, in fault tolerant system several identical actuators are used to make the system able to function in case of one actuator failure. This is the reason of having redundant system design for fulfilling the necessary condition of safety-critical system. In some cases, the additional actuators are not used for controlling the output variables to a reference value, but they are essential for meeting other performance benchmarks. For example, the incorporation of additional actuators may have the reason to constrain the system variables that may results in system efficiency or system dynamic performance. Using this feature of efficient performance in the context of overactuation, the aim of this thesis report is to address the optimized control strategy of overactuated 2DOF helicopter system for possible fast dynamics.

This feature of overactuation of a system can be used only if the system has more control inputs then the number of variables need to control to a desire reference point. Therefore, in an overactuated system there exist a set of control inputs that the control designers can use, which offer additional degree of freedom for performance optimazation. The advantage of additional degree of freedom make the control designers to design and modify the control strategy accordingly that accounts the dynamics of overactuation of the system. The real actuators in most cases have saturation limits beyond which it cannot make changes for a given control input. Therefore, these limitations should be considered for optimizing the system performance. The system methodology has to be practical while considering the actuators hard limitations. Optimization on a large scale will lead the system to slow response and become intractable despite its efficient simulation results.

The proposed helicopter system is a custom made over-actuated 2DOF Double Twin Rotor Aerodynamic system (DTRAS), a simplified version of helicopter, to investigate for possible fast dynamic responses. The intention of using this laboratory version of 2DOF helicopter system is to investigate the dynamics and control of a tandem rotor helicopter. While being quite simple this 2DOF system still offers a good simplification of a real world tandem helicopter for evaluating performance of different automatic control principles.

Even though the proposed mechanical construction and components used in helicopter model is very simple and interesting, there are some certain challenges regarding Control and components functional limitations. The researchers have investigated ways for developing and exploiting the features of vehicles dynamics for fast dynamics, but there are certain limitations on its performance, as its maneuvering competency depends on the performance of its motors. In other words, no matter how good the control algorithm is the vehicle performance will be as fast as the motors are. Fast transient dynamics in motors demand high peaks in current. Usually, the electrical motors found in such vehicles have its dynamics diminished and keep the peak current below levels of its saturation above which it would damage the vehicle circuitry or the motor coils. Then, due to the dependency of the performance of the vehicle on the motors dynamic performance, there exists a clear performance barrier. Therefore, new actuation strategy required to deal with the performance barrier face by motor. In this

work, taking advantage of the additional control inputs provided by the proposed overactuated helicopter system, control strategy been implemented for fast dynamics that uses additional actuator for controlling each degree of freedom. This new actuation strategy breaks the link between motor performance and vehicle performance.

The proposed helicopter system shown in is a laboratory version of the complete tandem helicopter system, stands and fixed to a vertical rod that restrict its motion about pitch and yaw axis of the system. This system uses two Brushless DC motors for controlling elevation motion and two other for controlling azimuth motion. This make the system overactuated having four control inputs for controlling two system's variables, i-e pitch and yaw angles.

This helicopter system is connected to an industrial PC googoltec act as a central control unit, in Automation laboratory of Mechatronics engineering in Kocaeli University. Professor Dr. Zafer Bingul is the core supervisor of this project. This project thesis covers the development process of following areas:

- Design of Vehicle and fabrication
- Estimation Using EKF
- System Integration and Testing
- Modelling and Simulation
- Control Strategies Design

The aims of this thesis report are (1) to design extended Kalman filter for system states estimation and (2) compare the controlled performance of the overactuated 2DOF helicopter using three different control algorithms. As the system is overactuated, this report is focusing more on the fast dynamics responses with increased control bandwidth using two extra actuators then the normal helicopter system. The main objectives are summarized as given below.

- Developing a new overactuation idea for fast dynamics responses by exploiting the maximum double thrust of two actuators (motors).
- IMU sensor used for measuring attitude states of the helicopter system. These measurements have noises (electrical noises and mechanical vibrations) related

with them. In order to filter-out these noises, an extended Kalman Filter designed for estimating nonlinear states of the helicopter system.

- A proposed 2DOF helicopter practical model is constructed. The pictorial view is shown in Figure 2.1.

- An actuation algorithm needed to allocate the control signals to the appropriate actuators to deal with redundancy.

- Helicopter dynamics analysis, mathematical modeling of the overactuation system, modeling of propulsion system and optimized controller design tested in simulation.

- The control architecture based on PID, Cascaded Full State Feedback control and Fuzzy Logic Control are implemented.

- Implementing and validating the simulated helicopter system and testing of real time trajectory tracking.

1. LITERATURE REVIEW

This chapter covers the previous literature work done about the helicopter systems by various researchers. In this chapter, four main subsystems of the proposed helicopter system are explained in context of previous work done in each area. These are given below as

- Helicopter Dynamic Modeling
- Propulsion System modeling
- Extended Kalman Filter
- Optimized Control allocation

In dynamic modeling of helicopter system, background works that develops the mathematical governing equations of the conventional helicopter's system are explained. Second, in propulsion system, the previous work on thrust force modeling are investigated and the resulted proposed design are presented. For state estimation of the helicopter dynamic states, first, a brief introduction about Kalman Filter is given and later, with its uses in helicopter system's context is explained. Lastly, in optimized control allocation, the optimized control allocation introduction is given and its advantages are outlined.

1.1. Helicopter History and Working principle

Helicopter is a machine with one main horizontal power driven propeller that make it possible to take off upright and land perpendicularly. Using this propeller or rotor, helicopter can travel in any direction and can hover.

The word's first flight of helicopter took place in Stratford, Connecticut on September 14, 1939. This helicopter named VS-300 was designed by Igor Sikorsky and the first helicopter include a single main rotor and a tail rotor scheme. This first helicopter design was built by Vought Sikorsky Aircraft Division of the United Aircraft Corporation [1,2]. The main rotor has 28 feet diameter of three blade provide a variable pitch of blades. The blades speed reaches to 250 to 300 mph. The concept explained

in [1] and demonstrated by VS-300, offers the fundamental idea for the first production helicopters. This conceptual design of helicopter became the standard for manufacturing companies across the world. The first patent [1], that explain the main technical features of the VS-300 was submitted by the Sikorsky on June 27, 1931. On March 19, 1935 the patent was approved and presented to Henry Ford and included in his Edison Museum in Dearborn, Michigan on October 7, 1943. In the Henry Ford Museum, the VS-300 is still on display [2]. There are many examples of UAV helicopter uses for commercial and security purposes. Such examples are HEF 32, Aeroscout, Unmanned Little Bird H-6U and Alpha 800 UAV as shown in Figure 1.1 below.
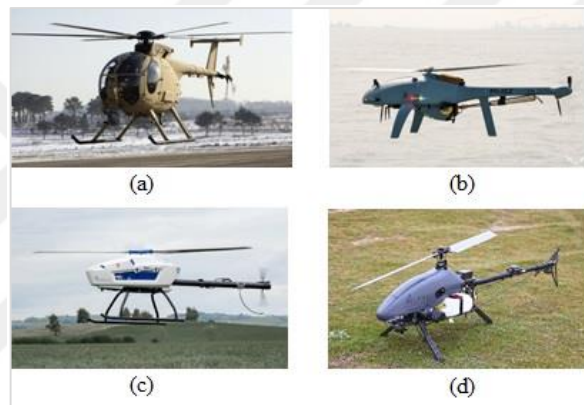
Figure 1.1. (a) Little Bird H-6U, (b) HEF 32,
(c) Aeroscout (d) Alpha 800.

The travel direction and various maneuvering movements of helicopter can be achieved by the systematic actuation of the main and tail rotors speed and orientations. As can be seen in Figure 1.2 below, the basic dynamic responses of the rotors make the helicopter to attain any required orientation.
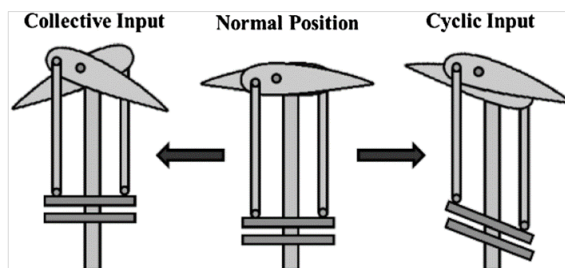
Figure 1.2. Collective and cyclic pitch

The helicopter lift is achieved by using the Collective Pitch which changes the angle of attack of the main rotor blades. This change in angle results in thrust force that lift the helicopter upward. The steering of helicopter sideways to a required direction can be achieved by making use of Cyclic Pitch which make a differential thrust forces of main rotor to turn the helicopter to a desire direction. The node of helicopter can be steer by changing the speed of the tail rotor.

1.2. Mathematical Modeling of Proposed System

The proposed helicopter design in this report is based on a Sikorsky configuration. In this arrangement the main rotor's axis is perpendicular to the tail rotor's axis. Both of the main and tail rotors systems are mounted on the rigid steel beam, acting as a fuselage. As explain before the main and tail rotors each consists of two brushless motor. All of the motors use the same size propellers having three rigid blades. The helicopter in space has six degrees of freedom, three translations along the X, Y, Z axes and three rotations around the same axes. The mathematical model for the proposed two degree of freedom is presented in this thesis report and is based on the previous works explained in [3-9].

1.2.1. Related work for mathematical modeling

Markus Ruf, in [7] uses an underactuated 3DOF laboratory helicopter platform Quanser, see [10]. This design model the travel, elevation and pitch control responses using two actuators. An indistrial based process of Model Predictive control used which is a numarical optimization algorithm. In [4], Michal Hoˇ modeled 2DOF tandem helicopter, Humusoft see [11], which investigate only the pitch and yaw control responses. The performances of designed model are compared using PID and modern methods of control regulators (LQ, LQG) and a linear states estimator, Kalman filter. [5] reports the dynamic model and control design for the underactuted 3DOF helicopter rig system. Along with LQR, it uses integral action and feedforward compensation for reducing the nonlinear effects. An extended Kalman filter is designed for measuring the unmeasured states of the control dynamics.

A lot of research have been performed on helicopter dynamics responses in context of its design configuration and the effects due to the external and internal disturbances.

Considering these factors that affects the behavior of helicopter during hover or heading states, researchers are trying to find way to model these disturbances accurately and design accurate responses for compensating these disturbances. In [12], Bouabdallah reports a primary justification and an inquiry of the main drivers behind the aerodynamics systems like quadrotors and helicopter. These early realization of helicopter dynamics is being followed by the plenty numbers of authors in their research. According to Bouabdullah's report in [12] the main effects acting on the aerodynamics vehicles are given in Table 1.1.

Table 1.1. Effects and its sources on helicopter dynamics

Effects	Sources
Gravity effect	Center of mass position
Gyroscopic effects	Change in orientation of the rigid body
	Change in orientation of the propeller plane
Inertial counter torques	Change in propeller rotation speed
Friction	All helicopter motion
Aerodynamic effects	Due to propeller thrust and its blade flapping

1.3. Propulsion System

Coaxial rotor system configuration has some advantage over single rotor system. It is more efficient in terms of endurance, payload capability and fast response in measurability. These leads encouraged the researcher both from military and civilian, to further investigate the performance of coaxial rotors propulsion system. The propose mechanism for propulsion system of helicopter require different electronic components, who's characteristics affect indirectly the thrust forces produce by brushless motors that use the control signal as an input.
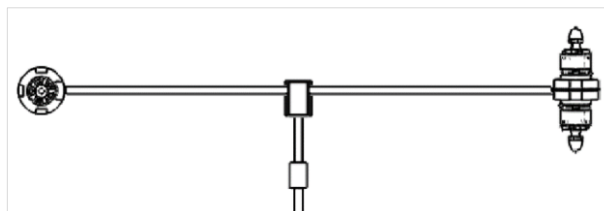
Figure 1.3. Pitch and yaw propulsive units

This project investigate coaxial rotor configuration with the aim of achieving fast dynamic responses of helicopter system by increasing the bandwidth and speed of actuaters and controls system. For this purpose a double dual twin rotor system is presented in this report that uses two actuatores for controlling a single DOF. This

mechanism is design with the intent to develop the vehicle robust propulsion mechanism and avoid excessive increase wind gust sensitivity. Using two propellers in one rotor also increases the existing rotor disk surface and cancel the counter torque effect. The general structure for the propose design of actuator system is shown in Figure 1.3 with chapter 3 explains in detail the modeling and response of the propulsion system.

1.3.1. Related work for propulsion system

In recent research [16] and [19] similar work investigated on twin rotor propulsion system (a multi-medium thrust mechanism) for a quadrotor that can demonstrate aerial and submersible flight under water. This development makes use of bio-inspired locomotion force analysis that make the vehicle capable both to fly in air and swim in water. Similar work on coaxial rotor for micro air vehicle is perform by S. Prothin in [18]. The thrust direction generated by two motors in propulsion unit can be change by tilting the propeller plane laterally and longitudinally using servos. This kind of thrust vectoring reduces unnecessary control surfaces that affect the vehicle's motion and become sensitive to crosswinds. In [14], a comprehensive experimental analysis of aerodynamics modeling of the propulsion system is been carried out. In these experiments the thrust forces and the aerodynamics drage forces are investigated for modeling part of propulsion system for dual axis tilt rotorcraft UAV. Similar comprehensive analysis of the aerodynamics modeling of helicopter is presented by J. Leishman in his book [13], in which a detail explanation is given about the aerodynamics behavior of helicopter rotor propeller. In this project, numerous experiments are carried out using momentum theory [17] to analyze the require characteristics of propeller to get an optimum response of propulsion system.

It is important for a simulation model to have a good approximation of each component that apply action on the airframe of the helicopter. In this project each DOF is controlled by two brushless motors with corresponding two drivers. A detail analysis in [15] is carried out on the dynamics of propulsion system components like brushless motor and speed controller. However, the results are not specifically applicable to this project but it offers the perception of its suitable use for the propose double twin rotor propulsion system in this project. The study of these components dynamics are helpful in understanding the response and system identification of drivers and motors.

1.4. Kalman Filter

A lot of publish work is available from various researcher explaining the working principle and mechanism of Kalman filter. Before referring to the literature about Kalman filter used in various applied worked of the kind resemble to this project, it is first useful to understand the basic notion of randomness. The quality or state of lacking a pattern or norm of organization is a term randomness. As [20] explains, randomness take place and is unavoidable in all walks of life. It is patternless but not propertyless. The sequence of random numbers the computer generates are deterministic ontology (nature of being) but for the users who do not know how these numbers are generating is probabilistic epistemology (understanding methods). This phenomena of randomness give us confidence to study the measured quantities of different properties of a matters that exhibits the phenomenon of randomness over a suitable space and time. Therefore, it is meaningful to add the effect of randomness (random noise) to the dynamics equations of motions. Investigating these effects will help us to simulate and ultimately implement the correct nature of the physical system using Kalman filter mechanism. In short, a Kalman filter is a recursive data processing algorithm that estimates the noisy (different sources) states of linear dynamic system.

The first theoretical formulation of Kalman filter was made by Rudolf Emil Kalman [33,34,40,41]. This filter mechanism uses discrete time linear dynamics model system that can be represented in a state space model. Where [35] gives the insight of estimation mechanism of Kalman filter by solving several real word estimation problems. Virtually the Kalman filter is been used in every technical or quantitative fields. For example, in engineering fields Kalman filter is use in the areas of tracking [23], fault detection [27], navigation and global positioning [21, 22], robotics [25], guidance [24], radar [26] and computer vision [28]. It is also utilized in applications involving signal processing [29], voice recognition [30], video stabilization [31], and automotive control systems [32].

1.4.1. Related work for Kalman filter

In [36], a modified form of EKF estimation algorithm is implemented which is based on the strapdown and bi-vector method to estimate the states of small helicopter from three sources. The strapdown method is used as states update and bi-vector estimation

as measurement update. Using Euler forward approximation and discretization of 3DOF helicopter dynamics model, an Extended Kalman filter is designed in [5]. Master thesis in [37,39], explains in details the use of Extended Kalman filter for controlling the attitude of UAVs. Using the predicted aerodynamic model data and the integrated sensor data, EKF is used to get the improved states of quadrotor. The Extended Kalman filter performance has been tested in a simulated environment model of the quadrotor system in Simulink platform. A military based short range Autonomous Underwater Vehicle (AUV) navigator system is designed in [38]. The aim of the project was to use inexpensive sensors and less digital processing time. In this report the results of a navigator are presented that uses the nonlinear model of the vehicle for Extended Kalman filter.

1.5. Control Allocation System

Control Allocation is a mathematical mechanism that distribute the control signal into separate actuator's required input signals. Therefore, it is an important tool for an overactuated system. The vehicle in this project is an overactuated system, therefore Control Allocation algorithm is used. In [42], O. Harkegard gives two steps for designing the control system in context of overactuated system considering Control Allocation mechanism.

- Designing a control signal for producing the require effort needed for require response.
- Designing the control allocator strategy that maps the total control signal to the individual actuators for separate require action on the system.
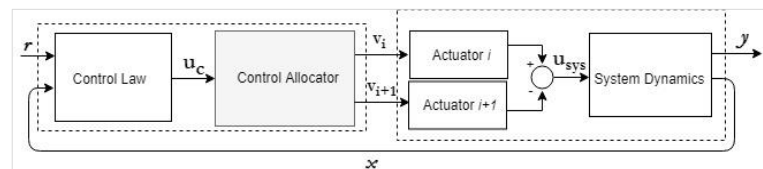
Figure 1.4. Control system design structure with control allocation

2. AERODYNAMICAL SYSTEM DESCRIPTION

This chapter covers the initial brainstorming performed about the physical design and fabrication steps involved for each component of 2DOF laboratory Aerodynamical system given a standard name of Double Twin Rotor Aerodynamic System (DTRAS). Also a brief introductions of avionics system that consist of basic helicopter system devices (sensors, cables, controller etc.), propulsion system components and power unit are discussed. Before developing the mathematical model for the proposed design of overactuted Aerodynamical system, it is first necessary to describe the visualized shaped and its dimensions. Therefore, this chapter manly focus on the design procedure of overactuated system.
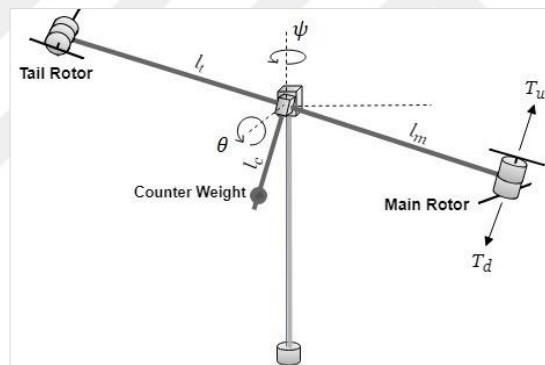
Figure 2.1. 2DOF DTRAS system

As chapter 1 explains in detail the concept of overactuation of physical system, this thesis accounts for the project of similar overactuated 2DOF DTRAS that explore an increase in performance compare to the conventional actuated helicopter system. In [43, 44], an actuated 2 rotor Aerodynamic systems are designed that resembles the behavior of actual helicopter with only 2DOFs. In this design, pitch motion can be achieved by controlling the speed of single main rotor having larger propeller compared to tail rotor, whereas yaw motion can be performed using both the effect of counter torque from main rotors and reacting tail rotors torque. This platform comprises of a circular cylinder shape beam act as a fuselage, pivoted at its uneven point on a vertical column of same shape and size, in such a way that it can freely make movements in vertical and horizontal plan, as shown in Figure 2.1.

2.1. Requirements and Specifications

The project requirements are to develop a 2DOF laboratory version of helicopter system. This system has pitch and yaw motion each require two motors to provide more agility in systems dynamics responses. Hence, compare to the design given in [43,44], the total control input variables in the proposed design becomes 4. Figure 2.2 shows the control signal flow for the actuating unit of DTRAS system.
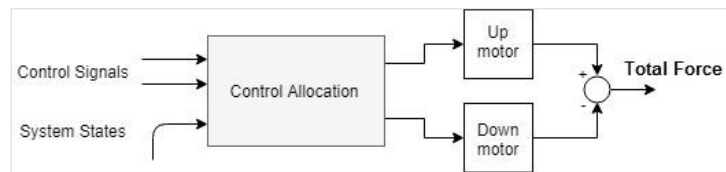
Figure 2.2. Control allocator signals for pitch motors

Specific design Consideration are:

- Each pitch and yaw motion use two motors connected coaxially with opposite thrust forces for quick forward and backward movement about corresponding axis (more details are given in the propulsion system modeling section in chapter 4).
- The pitch angle movement is constraints to -90 < theta < +90 degrees and yaw angle limits are 0 < phi < 360 degrees.
- The moment of inertia of helicopter body were kept high compare to the motors moment of inertia that makes the controls more challenging in achieving fast responses.

2.2. Aerodynamics System General Body Frame

- Steel bars of circular shape
- Central hub joint
- Mounting stand
- Dual Rotors Propulsion System

2.2.1. The steel bars

The steel bars of circular shape as shown in Figure 2.3, act as a fuselage.

Figure 2.3. Steel bars for main and
tail beam

The total length is divided into main beam and tail beam and joined by a central hub. The vertical column supported and hold by the mounting stand at the bottom. The dimensions of fuselage beams and column are given in Table 2.1.

Table 2.1. Aerodynamics System body frame dimensions

	Length (mm)	Diameter (mm)	Mass (g)	Moment of inertia (Kgm^2)
Main beam	266	7.85	155	1.1939E-6
Tail beam	242	7.85	145	1.1169E-6
Counter weight beam	203	7.85	80	6.1622E-7

2.2.2. The central hub

The central hub consists of Fuselage joint, Column joint and Pitch movement axle.
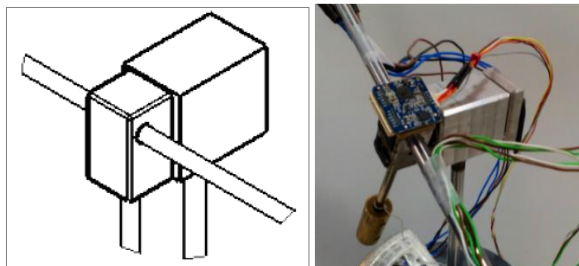
Figure 2.4. Central hub joint

The Fuselage joint is made by rectangular aluminum cylindrical shape object that joined the main beam, tail beam and Pitch movement axle. The Column joint is also a rectangular aluminum cylindrical shape object that joint the column bar and Pitch

movement axle. The Pitch movement axle is a circular cylinder that passes through Fuselage joint and Column joint. The pitch axis of DTRAS passes through this axle around which the DTRAS makes pitch movement. The geometrical shapes and dimensions of the Central hub are given in Figure 2.4 and Table 2.2 respectively.

Table 2.2. Central hub components dimensions

Item	Mass (g)	Dimensions (mm)
Pitch Joint Rectangular Cylinder	45	10x8x10
Yaw Joint Rectangular Cylinder	50	10x10x10

2.2.3. Mounting stand

The stand on which the whole DTRAS system is setup is shown in Figure 2.5. It consists of three discs with the bottom one of radius 10 cm and the upper two disc of radius 8 cm. These discs are firmly hold by four metallic circular bars of length 12 cm and radius 0.8 cm. The central steel bar is passed through the center of the discs using ball bearings. The down end is connected to the yaw encoder for measuring yaw angle.
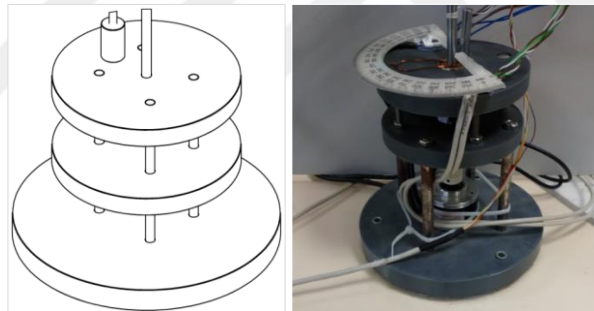
Figure 2.5. Mounting stand for 2DOF DTRAS

2.2.4. Dual rotors propulsion system

Unlike the conventional real size helicopter, the Double Dual Rotor Aerodynamic System, shown in Figure 2.6 below uses the propeller with fixed angle of attack that provide a constant thrust force for a given propeller (rotor) velocity. Therefore, the only control input signals are the voltages (PWMs) that determine the speed of propellers. [16] developed the same concept of homogenous twin-rotor propulsion system for UAVs which make the vehicle fly and swim in water, whereas [18] uses different rotors for flight and swimming purposes. In both cases due to multi medium thrust mechanism, the vehicles were capable of travelling in both air and water. The DTRAS system uses two Dual Rotor Propulsion units with same dimensions and same

characteristics, which is the case similar to [16]. These units are connected at the ends of main and tail beams of fuselage in such a way to control the pitch and yaw movements of the DTRAS system respectively. A single Dual Rotor propulsion unit, consists of following parts:

- Two motors
- Motor holder
- Motors mounting bed
- Propellers
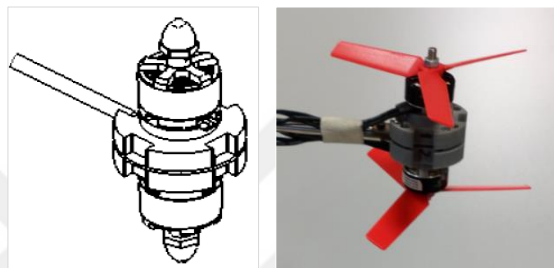
Figure 2.6. Single twin rotor propulsive unit

The motors mounting beds are connected with each end of main and tail beams. The two motors holders with motors fixed on them then connected with mounting bed on the ends of each main and tail beam using light weighted screws. The whole pitch and yaw propulsion systems assembly along with its orientation on fuselage is shown in Figure 2.7.
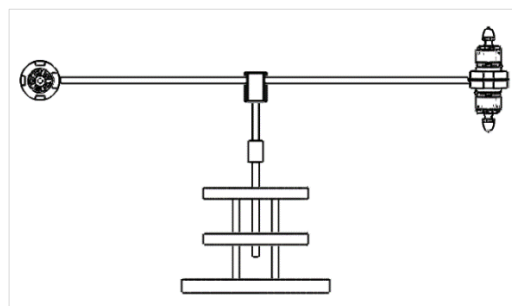
Figure 2.7. Double dual rotor represents pitch and yaw propulsive units

2.3. Motors

There were several options for choosing motor for propulsion system in market. Since the propose DTRAS system uses heavy structure of metal beams, it was necessary to use light weighted and more powerful motor that can provide needed thrust using

appropriate propellers. Two motors [45, 46], were studied considering the DTRAS systems needed requirements. The Tiger Motors F40 pro, [46], shown in Figure 2.8 was the most appropriate options available in market due to its low weight and more output power.

Table 2.3. Tiger F40 Pro motor specifications

Internal Resistance (mΩ)	31.5
Shaft Diameter (mm)	4
Weight with cable (g)	31.7
Dimensions (mm)	Φ27.9x30
Voltage Range (V)	10-16
Maximum Power (W)	690
Idle Current (A)	1.7
Maximum Current (A)	45

The technical specifications are given in Table 2.3. This motor can provide upto 690 W of power and maximum thrust of 1563 G, that require for achieving fast responses which is the goal of this project.

Figure 2.8. Tiger F40
Pro brushless motors

Some researchers have carried out practical static experiments in [48] and reviews in [49]. These experimental data provided by the manufacturer in Table 2.4 is carried out using 5045 3-Blade standard propellers.

Table 2.4. T-Motor F40 PRO 2400KV manufacturer experimental data

Model	Volts (V)	Propeller	Throttle (%)	Current (A)	Watts (W)	Thrust (G)	RPM	Efficiency (G/W)
F40 PRO 2400kv	15.4	5045 3-Blade propeller	55	12.8	202.84	639.32	18293	3.15
			65	19.05	300.15	825.67	20683	2.75
			75	23.87	374.38	1003.68	22853	2.68
			85	31.52	490.55	1186.75	24985	2.42
			95	35.64	551.35	1293.31	25900	2.35
			100	44.9	689.22	1562.69	28390	2.27

However, more experimental analysis for designing propulsion system using the responses of static and dynamics experiments of these motors are performed in chapter 3, where a comprehensive practical experiments are documented. A general full description of motor selection procedures is studied and mentioned in Al Rihani's thesis [47].

2.4. ESCs

Electronics Speed Controller (ESC) is a brushless motors driver mostly used for speed controlling. It can also be used for changing direction of motor rotors rotation. In a broader concept it is a pulse width modulation controller act as a driver for electric brushless motors. The important consideration should be keep in mind, which is the match of ESC choosing for the specific brushless motor.
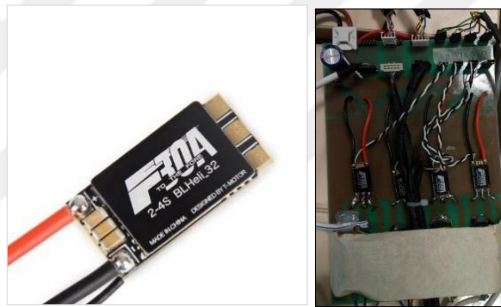
Figure 2.9. F30A ESC and custom made board

In this project a most suitable and matching ESCs, F30A, designed by T-motors are been chosen. These ESCs are able to withstand 30A of continuous current and 40A of burst current with maximum of 16V (Lipo 2-4S) as an input DC voltage. The complete manual and use of F30A in different configuration is described in [50]. Whereas, in [51], the precaution and calibration procedures are for explained generally. In Al Rihani thesis [47] a full description for the selection process is explained. The motor controller is shown in Figure 2.9.

Table 2.5. F30 A ESC specifications

Current Capacity (A)	30
Voltage Range (V)	10-16
Weight (g)	5.7
Dinemsions (mm)	25.5x12.7x5

2.5. Controller

The GT-800 series motion controller as shown in Figure 2.10, is an 8-axis controller which provides more control axes and functionalities than its previous model, GT-400 series. Providing high-performance and flexibility, the GT-800 is applicable to the control of multiple-axis equipment such as PCB drilling and milling machines. However, this controller is used for controlling the 2DOF DTRAS system. It uses C/C++ function library which is most suitable to program for controlling the plant. The control block circuit includes an Industrial PC Controller, GoogolThech GT-800 Series Motion Controller and a custom made PWM Generator card as shown in Figure 2.15 which uses ATMEGA128 microcontroller which handles the main task of converting and regulating the control system signals.

Figure 2.10. Googoltec controller

Following are the main features of the GoogolThech GT-800 controller.

- Adopt high-performance DSP and FPGA technology.
- Each card can control 8 servo/step motors.
- Sampling period is programmable. The minimum interpolation period of eight axes is 400μs. The minimum control period of single-axis motion is 25 μs.
- Motion mode: point-to-point motion, linear interpolation, circular interpolation, velocity control, manual pulse generator interface, and electrical gear. Programmable T-curve planning and S-curve planning. On-the-fly update motion control parameters.
- All the position and parameter registers are of 32 bits.
- Hardware capture home switch and index signal of encoder.
- Set following error limit, acceleration limit and output limit, to ensure safe and reliable control.

- PID (Proportional-Integral-Derivative) digital filters with velocity and acceleration feed-forward, and integral limit and output bias compensation.

The technical specifications include hardware, software and the list of the require accessories that include input/output board, terminal board and cables are mentioned in appendix B.

2.6. GT-800-ACC2 Terminal Board.

This Terminal board act as an interface between GoogolThech controller ports and the plants input/output connections. It has a set of standard ports like DE 9F, DE 9 Serial RS232 and DB 25 Serial/COM ports, distributed among 18 channels. Also, there are manual flexible connectors uses for sensors or switching purposes.

Figure 2.11. GT-800 terminal board

2.7. Propellers

There are alot of different kind and size of propeller available in market. To avoid high frequencies of vibration, Gemfan 5-inch 3D 3 blade propeller were chosen as shown in Figure 2.12. These propellers are use specifically for multi-rotor drives which make the motor capable of creating thrust forces in two directions. However, this project only focuses on control algorithms that involve one direction thrust force generation by each motor. Moreover, due to its small size diameter with symmetric inertia distributed about its axis of rotation, it provides a uniform thrust force without creating excessive increase in wind gust sensitivity. Hence, at low to high angular speed, these propellers avoid high frequencies of vibration. The technical details of the chosen propellers are given in below Table 2.6.

Table 2.6. Propeller specifications

Manufacturer	GemFan
Size (inch)	5 (3 Blade 3D)
Hub Size (mm)	5
Pitch (inch)	4.6
Weight (g)	4.85
Model	RCX01-658

In Al Rihani thesis, [47], a full procedure is explained for selecting appropriate propellers for a specific motor.

Figure 2.12. Gemfan 5-inch 3D 3 blade propeller

2.8. Sensors

Sensors are essentials parts in control system for taking feedback to the controller to correct the actuating signal by apply specific control laws. In this project two set of sensors are used for investigation the response of the system. An embedded unit that consists of several sensors called Inertial Measurement Unit IMU and discrete type position encoders each for pitch and yaw motion reading.

2.8.1. IMU sensors

There are several range of choices available for IMU sensor in market. All of them have very small difference in performance. The UM7 [51], is a 3rd-generation Attitude and Heading Reference System (AHRS) that takes advantage of state-of-the-art MEMS technology to improve performance and reduce costs. The UM7 combines triaxial accelerometer, rate gyro, and magnetometer data using a sophisticated Extended Kalman Filter to produce attitude and heading estimates.
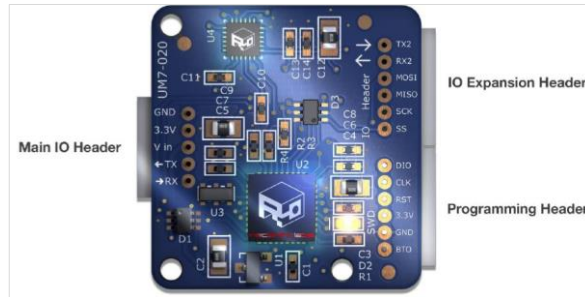
Figure 2.13. UM7 inertial measurement unit

The UM7 also adds many new features, including higher gyro bias stability and lower noise, a new communication architecture for improved flexibility, optional NMEA packet transmission, UTC time-synchronization with external GPS, and support for third-order temperature compensation on all sensors. The UM7 comes with one 5-pin cable assembly for the main IO header. A USB expansion board is available to make it easy to connect the UM7 to your computer. It can then use the CHR Serial Interface [51] to configure the sensor, and view and log data in real-time. Figure 2.13 shows the picture of UM7 IMU and Table 2.7 shows specific characteristics.

Table 2.7. UM7 IMU specifications

Vin	5.0 V
Baud Rates	9600, 14400, 19200 38400, 57600, 115200, 128000, 153600, 230400, 256000, 460800, 921600, default 115200
Communication	3.3V SPI bus, 3.3V TTL UART
Power consumption (W)	0.25
Dimensions (inch)	1.06x1.02x0.26
Data output Rate (Hz)	1-255
Operating Temperature (^{o}C)	-40-85
Weight (g)	11
Output Data	Attitude, Heading Attitude quaternion GPS attitude, position, velocity GPS position in meter from home position Raw mag, accele, gyro data Calibrated mag, accele, gyro, temperature data

2.8.2. Encoders sensors

In order to verify the estimated output attitude information from the extended Kalman filter, the encoder sensors for pitch and yaw position measurement are used. For pitch position measurement, HEDS-5500 shown in Figure 2.14, is an optical type encoder with 256 pulses per revolution is used. Yaw motion is measured using HE50B series incremental encoder, shown in Figure 2.14 is used with output of 300 pulses per

23

revolution. The technical specifications, electrical connections and geometrical diagrams of both encoders are given in appendix A.
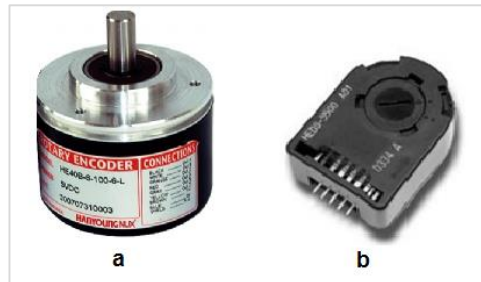
Figure 2.14. (a) HE50B yaw encoder,
(b) HEDS5500 pitch encoder.

The pitch and yaw positions and velocities information are measured using two encoders each for pitch and yaw position measurement and IMU sensors at the same time. The IMU data are then estimated using extended Kalman filter and compared with the same information measured using encoders as shown in Figure 3.21 and Figure 3.22. The calculated raw data measured before processing through extended Kalman filter is shown in Figure 3.19.

2.9. Signal Processing Board

The figure shown in Figure 2.15, is a custom made signal processing board, uses ATMEGA128 microcontroller which handles the main task of converting and regulating the control system signals. The main features include, variable power supply, ranges from 5-12V, analog to digital (A/D) and digital to analog (D/A) converters, serial communication port uses DE 9F, DE 9 serial RS232 and encoder connections.

In this project, four brushless DC motors are employed which uses electronic speed controller (ESC) as a driver. This driver uses analog signal ranges from 0-5 volts. The GoogolThech controller provides analog signals for actuating the motors. Therefore, this analog signals need to be converted to a PWM signal with voltage ranges 0-5V. The AVR controller in signal processing board uses the timer and A/D converter IC to modulate this analog signal received from GoogolThech controller to the required

PWM signal. This PWM signal act as an input to the ESC that drive the brushless DC motor.
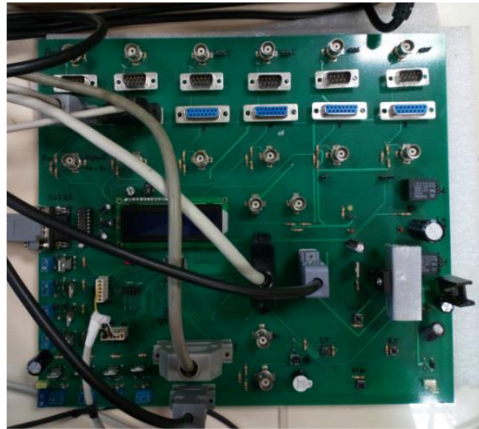
Figure 2.15. Signal processing board

The complete generalized schematic that shows the function of each component and signal flow is shown in Figure 2.16.
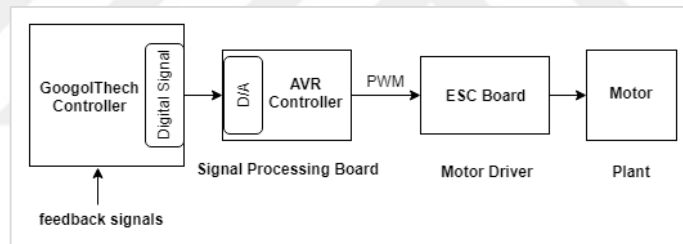
Figure 2.16. Generalized signal flow of the DTRAS system

3. MODELING

This chapter covers the development of various subsystems modelling of 2DOF DTRAS that consists:

- Mathematical Model of Vehicle
- Aerodynamic modeling of Vehicle
- Gravity Compensation
- Design of Extended Kalman Filter

The objective of modeling of the physical system is to analyze the performance of the system before designing the actual control system. The mathematical modeling includes the development of physical equations representing the dynamic of the 2DOF Aerodynamic System. All the parameters are defined and measured physically for developing the mathematical model. The free-body-diagram is given for visualizing kinematics and understanding the effects of forces and moments on vehicles that effects its motions. These analyses are performed using Euler-Lagrange formalism to developed the require physical differential equations and test the performance first in Matlab Simulation of the instable system.

Second, the Helicopter is a highly non-linear mechanical system that generates various bodily effects like from aerodynamical and mechanical domains. Therefore, the modeling of the vehicle dynamics need to considered such effects. The list of main effects is mentioned in Table 1.1 in chapter 1. The aerodynamic modeling involves the analysis of the thrusts and the aerodynamic drag torque applied on the vehicle, since these are the only dominant forces and moments. The main components that are responsible for the thrusts forces and moments generation are propellers, motors and ESCs.

In order to analyze the performance of the propulsion system, the propeller aerodynamic thrusts forces and drag moments are calculated experimentally. The data obtained from the experiments shows the propeller characteristics are accurately modelled by calculating the thrust and torque constant coefficient. The motors used in

this prototype is investigated for its suitability by carrying a series of static experiments that shows its performance viewing the calculated efficiency. Also, the behavior of the motor in a dynamic analysis is investigated by performing dynamic experiments to find its transfer function in time domain. The dynamic analysis for the actuator is important for creating an accurate model in designing the control law for the whole system. Similarly, ESC, the motor controller is also analyzed in order to show its linearity for a range of input voltage variations. The following assumption are taken while developing the mathematical model and simulation.

- The vehicle frame is considered rigid
- The propellers are rigid
- Thrust and drag forces are proportional to the square of the propellers speed
- The Center of gravity and the vehicle body fix frames origin are not coincident

3.1. Kinematics

The method of representing the rotation of rigid bodies in space involve Euler angles, Tait-Bryan angle and Quaternions. These methods use the projection of sensors actual values on the frame of interest to represent the real value experience by the physical system subjected to require orientation. Quaternions are more powerful way of representing orientation in space as it effectively handles the problem of gimbal lock when the pitch angle goes beyond 90 degrees. In case of the proposed 2DOF DTRAS system, the pitch angle is restricted to 85 degrees. This constraint let us the use of Euler angles in representing the orientation of vehicle.

Euler angles uses a combination of three successive rotations about a particular axis to represent the object complete orientation. The process of sequential rotations makes use of multiple coordinate frames each have its own rotation about a particular axis. Normally the transformation is carried out from body frame to inertial frame.

3.1.1. Body frame:

The body frame is represented by the physical axis for a particular IMU according to which various sensors are places. For simplicity, in most of the cases, the sensors body frame is aligned with the systems body reference frame.

3.1.2. Inertial frame

The inertial frame is an Earth fix frame whose axis are fixed with Earth frame axis. This frame is an unmovable frame representing the aeronautical inertial reference frame in which if x-axis represents the positive heading of the vehicle, the positive y-axis shows the right side and the positive z-axis is directed down. This is also called North- East-Down reference frame.

Now considering the right-hand oriented coordinate frame, the method of Euler angles representation involve the three angles successive rotation describe separately as follow:

- $R(Z,\psi)$ represents rotation about z-axis
- $R(Y,\theta)$ represents rotation about y-axis
- $R(X,\varphi)$ represents rotation about x-axis

Theses matrices are represented by following matrices,

$$R(Z,\psi)=\begin{bmatrix} \cos\psi & \sin\psi & 0 \\ -\sin\psi & \cos\psi & 0 \\ 0 & 0 & 1 \end{bmatrix} \tag{3.1}$$

$$R(Y,\theta)=\begin{bmatrix} \cos\theta & 0 & -\sin\theta \\ 0 & 1 & 0 \\ \sin\theta & 0 & \cos\theta \end{bmatrix} \tag{3.2}$$

$$R(X,\varphi)=\begin{bmatrix} 1 & 0 & 0 \\ 0 & \cos\varphi & \sin\varphi \\ 0 & -\sin\varphi & \cos\varphi \end{bmatrix} \tag{3.3}$$

The resultant rotation matrix is a transformation matrix obtained by proper order multiplication of the previous three matrices. The resultant rotation matrix for moving from inertial frame to body frame can be form the following order of multiplication of above matrices with ignoring the axis name in the argument of each matrix. The order of rotation is illustrated in the following relation.

$$R_i^b(\varphi,\theta,\psi)=R(\varphi)R(\theta)R(\psi) \tag{3.4}$$
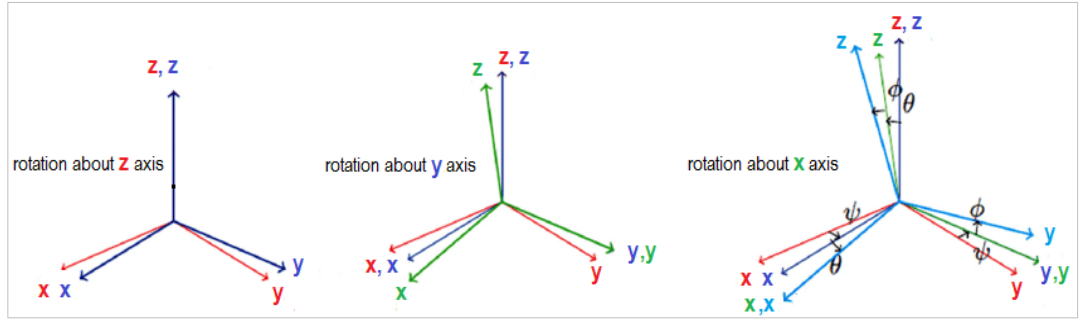
Figure 3.1. ZYX order rotation of Euler angles

In opposite direction, from body frame to inertial frame the resultant rotation matrix is given by

$$R_b^i(\varphi,\theta,\psi)=R(-\psi)R(-\theta)R(-\varphi) \tag{3.5}$$

This can be done by reversing the order of operations and also reverse the direction of rotation.

3.2. Angular Rates

The angular rates are measured physically by using gyroscopes in IMU sensor. Therefore to get the measured physical angular rates the transformation matrix calculated above can be used to transform the gyros rates $[p\ q\ r]$ to $[\dot{\varphi}\ \dot{\theta}\ \dot{\psi}]$, where this transformation matrix is given by

$$D(\varphi,\theta,\psi)=\begin{bmatrix} 1 & \sin\varphi\tan\theta & \cos\varphi\tan\theta \\ 0 & \cos\varphi & -\sin\varphi \\ 0 & -\sin\varphi/\cos\theta & \cos\varphi/\cos\theta \end{bmatrix} \tag{3.6}$$

However, the proposed 2DOF DTRAS system uses only pitch and yaw angles for its orientation. This make the system to move about pitch axis y and yaw axis z as shown in Figure 3.2. The resultant Euler rates can be calculated using the following relation for the system represented in Figure 3.2.

$$\begin{bmatrix} \dot{\varphi} \\ \dot{\theta} \\ \dot{\psi} \end{bmatrix}=D(\varphi,\theta,\psi)\begin{bmatrix} p \\ q \\ r \end{bmatrix} \tag{3.7}$$

Here, p=φ=0 as there is no roll motion involved in the system.

29

3.3. Angular Acceleration

The angular acceleration is calculated by time derivative of the angular rates of IMU sensor. Using the difference of two consecutive angular velocities $\partial\omega$ reading and the difference of its corresponding time ∂t from IMU, the ratio $\frac{\partial\omega}{\partial t}$ gives the angular acceleration. Because of system components vibration and variable loop time of IMU sensor the resultant angular acceleration is noisy. For this noise filtration, a naïve filter algorithm is designed. This algorithm is explained in section 3.10.4.
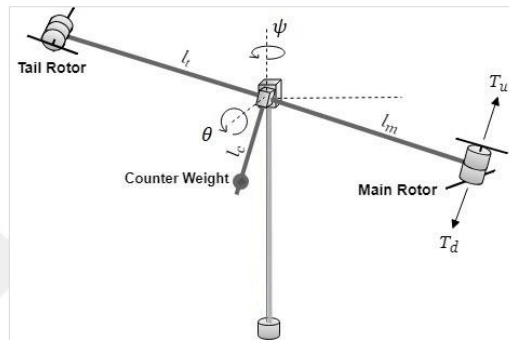
Figure 3.2. Kinematic of pitch and yaw motions

3.4. Mathematical Modeling of Vehicle Rigid Body

The free body diagram of pitch and yaw motion dynamics of proposed helicopter model given in Figure 3.3 and Figure 3.4 respectively.

3.4.1. Pitch motion dynamics
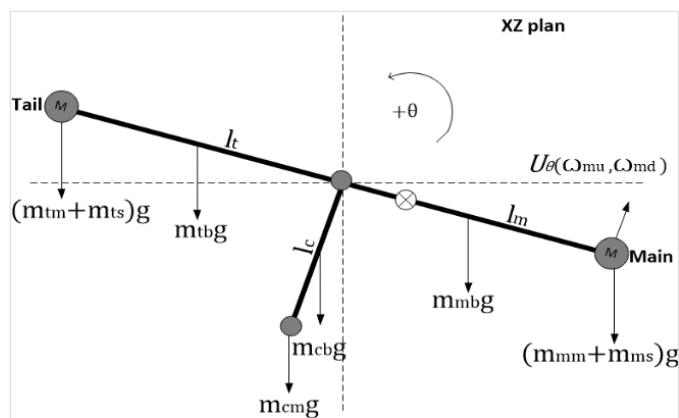
Figure 3.3. Free body diagram in pitch plan

The dynamic equation of the helicopter for pitch motion described as follow.

$$J_\theta\ddot{\theta}=E_{mtb}+E_{cb}-E_T-E_{cg}-E_f \tag{3.8}$$

Where J_θ is the inertia moment of the system about y horizontal axis, E_{mtb} is the torque due to gravity, the torque due to the net thrust force provided by main rotor is E_T, the centrifugal force torque is E_{cg} and torque due to friction force is E_f. Following are the relation given by equation (3.8).

$$J_\theta=El_t^2+Fl_m^2+Gl_c^2 \tag{3.9}$$

Where $E=\frac{m_{tb}}{3}+m_{tm}+m_{ts}$, $F=\frac{m_{mb}}{3}+m_{mm}+m_{ms}$ and $G=\frac{m_{cb}}{3}+m_{cm}$

$$E_{mtb}=(Al_t-Bl_m)g\cos\theta \tag{3.10}$$

Where $A=\frac{m_{tb}}{2}+m_{tm}+m_{ts}$ and $B=\frac{m_{mb}}{2}+m_{mm}+m_{ms}$

$$E_{cb}=Cl_cg\sin\theta \tag{3.11}$$

Where $C=\frac{m_{cb}}{2}+m_{cm}$

$$E_T=U_\theta l_m \tag{3.12}$$

Where $U_\theta=\chi_u(\omega_{mu})-\chi_d(\omega_{md})$

$$E_{cg}=D\dot{\psi}^2\sin2\theta \tag{3.13}$$

Where $D=\frac{m_{tb}l_t^2+m_{mb}l_m^2}{8}+\frac{m_{tm}l_t^2+m_{mm}l_m^2+m_{ts}l_t^2+m_{ms}l_m^2}{2}$

$$E_f=\dot{\theta}k_p \tag{3.14}$$

3.4.2. Yaw motion dynamics

The yaw motion of helicopter system is governing by,

$$J_\psi(\theta)\ddot{\psi}=A_T-A_f \tag{3.15}$$
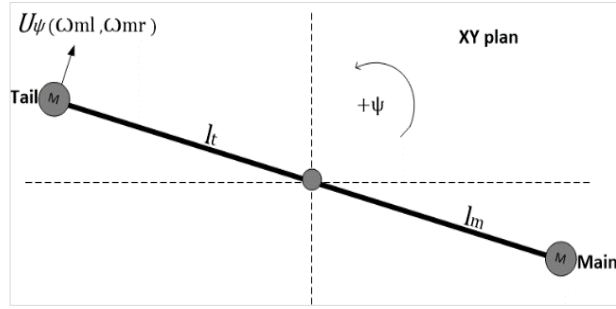
Figure 3.4. Free body diagram in yaw plan

In (9) $J_\psi(\theta)$ is the inertia moment of the system about z vertical axis, which varies with pitch angle θ, A_T is the tail rotor driving torque and torque due to friction force is A_f. The following relations holds for equation (3.15).

$$J_\psi(\theta)=\left(Fl_m^2+El_t^2\right)\cos^2\theta+Gl_c^2\sin^2\theta \tag{3.16}$$

Where F, E and G are the same that hold for equation (3.9).

$$A_T=U_\psi l_t\cos\theta \tag{3.17}$$

Where $U_\psi=\chi_r(\omega_{tr})-\chi_l(\omega_{tl})$

$$A_f=\dot\psi k_y \tag{3.18}$$

3.5. State Space Representation

Following the development of pitch and yaw governing equations, given by equation (3.8) and (3.15) respectively, the state space model of the nonlinear system is derived and presented below.

$$\dot x=f(x,u)$$
$$\tag{3.19}$$
$$y=g(x)$$

Where x is the state vector, u is the control input vector and y is the output vector. The choice of building the state vector by selecting the state variables are given below.

$$x_1=\theta$$
$$x_2=\dot\theta$$
$$\tag{3.20}$$
$$x_3=\psi$$
$$x_4=\dot\psi$$

Setting the state variables in sequence as given in equation (3.20), the state space model is presented as:

$$\dot{x}_1 = x_2$$

$$\dot{x}_2 = \frac{(Al_t - Bl_m)g\cos x_1 + Cl_{cb}g\sin x_1 - U_\theta l_{mm} - Dx_4^2\sin 2x_1 - x_2 k_p}{J_\theta}$$

$$\dot{x}_3 = x_4$$

$$\dot{x}_4 = \frac{U_\psi l_{tm}\cos x_1 - x_4 k_y}{J_\psi(x_1)}$$

(3.21)

3.5.1. Linearization

In order to design and investigate for control analysis, the state space model derived in equation (3.21) need to linearized about an equilibrium point. The equilibrium point can be found by setting $\dot{x} = f(x,u) = 0$, which is a steady state of the system.

$$0 = x_2^o$$

$$0 = \frac{(Al_t - Bl_m)g\cos x_1^o + Cl_{cb}g\sin x_1^o - U_\theta^o l_{mm} - Dx_4^{o2}\sin 2x_1^o - x_2^o k_p}{J_\theta}$$

$$0 = x_4^o$$

$$0 = \frac{U_\psi^o l_{tm}\cos x_1^o - x_4^o k_y}{J_\psi(x_1^o)}$$

(3.22)

Solving for the state variables give us the following values of $x_2^0 = 0$, $x_4^0 = 0$ and leave the following relation to solve:

$$0 = (Al_t - Bl_m)g\cos x_1^o + Cl_{cb}g\sin x_1^o - U_\theta^o l_{mm}$$

$$0 = U_\psi^o l_{tm}\cos x_1^o$$

(3.23)

This system has two equations and three unknown, which implies that there are many possible solution exists. Therefore, to solve for the unknown variables, one of the variable need to give an arbitrary value. Analyzing the second equation of system of equation (3.23), x_1^o, or U_ψ^o can be set to zero. The most suitable choice is to set x_1^o to zero, which gives:

$U_\psi^o=0$, $U_\theta^o=\frac{(Al_t-Bl_m)g}{l_{mm}}$ and x_3^0 is not appeared in the system which suggest that it does not have any effect at all. The second equation of system of equation (3.23) has an importance that tell us the fact that what amount of thrust force is require to hold the system pitch position to zero degrees.

Table 3.1. Steady state equilibrium point

x_1^o	0 degrees
x_2^o	0 degrees/s
x_3^o	0 degrees
x_4^o	0 degrees/s
U_θ^o	0.746 N
U_ψ^o	0 N

3.5.2. Linearized state space model

Following the selection of equilibrium point, it is now possible to present the complete linearized state space model of the proposed system in the form given below.

$$A=\frac{\partial f}{\partial x}(x^o,u^o)=\begin{bmatrix} 0 & 1 & 0 & 0 \\ \frac{-Cl_c g}{J_\theta} & \frac{-k_p}{J_\theta} & 0 & 0 \\ 0 & 0 & 0 & 1 \\ 0 & 0 & 0 & \frac{-k_y}{J_\psi(\theta)} \end{bmatrix}$$

$$B=\frac{\partial f}{\partial u}(x^o,u^o)=\begin{bmatrix} 0 & 0 \\ \frac{-l_m}{J_\theta} & 0 \\ 0 & 0 \\ 0 & \frac{l_t}{J_\psi(\theta)} \end{bmatrix} \qquad (3.24)$$

$$C=\frac{\partial g}{\partial x}(x^o,u^o)=\begin{bmatrix} 1 & 0 & 0 & 0 \\ 0 & 1 & 0 & 0 \\ 0 & 0 & 1 & 0 \\ 0 & 0 & 0 & 1 \end{bmatrix}$$

$$D=\frac{\partial g}{\partial u}(x^o,u^o)=\begin{bmatrix} 0 & 0 \\ 0 & 0 \\ 0 & 0 \\ 0 & 0 \end{bmatrix}$$

$$\begin{bmatrix} \dot{x}_1 \\ \dot{x}_2 \\ \dot{x}_3 \\ \dot{x}_4 \end{bmatrix} = \begin{bmatrix} 0 & 1 & 0 & 0 \\ \dfrac{-Cl_c g}{J_\theta} & \dfrac{-k_p}{J_\theta} & 0 & 0 \\ 0 & 0 & 0 & 1 \\ 0 & 0 & 0 & \dfrac{-k_y}{J_\psi(\theta)} \end{bmatrix} \begin{bmatrix} x_1 \\ x_2 \\ x_3 \\ x_4 \end{bmatrix} + \begin{bmatrix} 0 & 0 \\ \dfrac{-l_m}{J_\theta} & 0 \\ 0 & 0 \\ 0 & \dfrac{l_t}{J_\psi(\theta)} \end{bmatrix} \begin{bmatrix} U_\theta \\ U_\psi \end{bmatrix} \tag{3.25}$$

$$y = \begin{bmatrix} 1 & 0 & 0 & 0 \\ 0 & 1 & 0 & 0 \\ 0 & 0 & 1 & 0 \\ 0 & 0 & 0 & 1 \end{bmatrix} \begin{bmatrix} x_1 \\ x_2 \\ x_3 \\ x_4 \end{bmatrix} + \begin{bmatrix} 0 & 0 \\ 0 & 0 \\ 0 & 0 \\ 0 & 0 \end{bmatrix} \begin{bmatrix} U_\theta \\ U_\psi \end{bmatrix}$$

3.6. Aerodynamics modeling:

This section presents the analysis of aerodynamic forces and their moments require for dynamic motions of the helicopter system. Since the helicopter body frame has small area, the drag forces of the body are of small magnitude as compare to the thrust forces of the propulsion system. Therefore, the helicopter body frame's drag forces were neglected with only focusing on the aerodynamic response of the propulsion forces and its moments.

The main moments and aerodynamics forces applied on the vehicle are the torques and thrusts forces. Modeling theses dynamic characteristics require the classical method uses in aerodynamical engineering are used. These characteristics are explained by relations with dimensionless constants that develop the dynamic behavior of one quantity relative to other. The similar work on analyzing the aerodynamics properties are carried out in [14,53].

3.6.1. Aerodynamics analysis

For analyzing the physical system of 2DOF Aerodynamical system, it was necessary using MatLab simulation in order to model the thrust forces of propulsion system and compare that with the real physical thrust forces. Figure 3.6 shows the complete setup for measuring the thrust forces and torques generate by motor-propeller set. These data are then used for finding thrust force and torque coefficient represented by C_T and C_Q and are given by below equation (3.26) and (3.27) respectively.

$$T = \rho A(\omega R)^2 C_T \tag{3.26}$$

$$Q = \rho A(\omega R)^2 R C_Q \tag{3.27}$$

Here, ρ is the air density, A is the area of the propeller making disk, ω is the angular velocity of the propeller, R is the radius of the propeller disk.

Generally, in designing propulsion system of UAVs, static analytical measurements are carried out to find these trust forces and torque coefficients for specific propeller. Similar procedure is explained in details for analytical calculation of C_T and C_Q in [54,55]. These studies involve the measurements based on the idea of Momentum and Blade Element Theory. This theory is a simple method for investigating the propeller performance in which the blade is divided into a number of sections along its length. Each section is subjected to force laws for lift and drag measurements that results in thrusts and torque generation. Then at the same time the axial and angular momentum is applied for balancing that gives number of nonlinear equations. These solved equations then give the resulting thrusts and torque values for all the sections which show the performance of propeller. Another method involved in calculating propellers performance is Vortex Theory of Screw Propellers by Goldstein. These theories require an extensive work on the geometrical description of propeller's blade.

Figure 3.5. Components for static
torque and force testing

Since this project is mainly focuses only on estimation and control of 2DOF DTRAS system, working out these theories are itself an extensive and challenging area. Therefore, it was decided to experimentally measure the various characteristics for the chosen propeller. The experimental facilities include the electronics balance, weights,

string and tachometer. The whole setup for performing static analysis is shown in Figure 3.5. The main trust generating component is the brushless DC motor in the proposed 2DOF DTRAS System. In this section two main tests, static and dynamic, are conducted for the motor actuator.

3.7. Propulsive Group Modeling

The propulsive group of the 2DOF Aerodynamical System consists of Brushless DC motors, propellers and Electronic Speed Controller ESC. In order to analyze the performance of the propulsion system two tests, static and dynamic, are performed that study the response of the motor in the propulsion group. The static test was carried out to find the related parameters for the variables that characterize the behaviors of motor and propellers with input voltage in its operation. The Dynamic test on the other hand, performed to see and find the real behavior of combine components of the propulsive group. The result of this dynamic test helps in representing the real function of the motor in overall system simulation.

To assess the performance and its suitability of the motor selected for this project, various specification and characteristics are needed to consider for optimal operation. The motor selected for this project is F4 tiger motor and the complete manufacturer details are given in chapter 3. However, this details specifications are measured for 15 Volts of motor operation. In this project these motors are operated on 12 Volts of main power supply. Therefore, it was needed to measure the related specification and require characteristic for 12 Volts main power supply.

3.7.1. Motor static testing

As explained above the static test are performed to analyze the propeller response by finding the aerodynamic coefficients of thrust force, C_T and torque coefficient C_Q. Therefore, two static tests are performed each for motor thrust force and motor torque. The main objectives of static tests are:

- Investigate the propellers characteristics by finding the aerodynamic coefficients of trust force C_T and torque C_Q.
- Studying the linear behavior of the motor and its controller ESC.

- Calculate the efficiency of the propulsion system.

The components and its specifications use in these tests are mentioned in chapter 3.

3.7.1.1 Motor static test for thrust calculation

In this static test, the thrust force (g), current draw by motor in ampere and speed of the propeller is recorded against the input voltage in the form of PWM (%). Finally, relation is plotted between input PWM (%) and thrust force (g).

Now, to find the thrust force of the propulsion group the proposed prototype model is used. As shown in Figure 3.6 the propulsion group is attached at one end of the main beam and in similar way with equal distance from the pitch axis at the other end of the tail beam an inelastic wire is attached. This wire is then drawn downward vertically and attached with a 500 g weight and placed above the balance. The balance has a resolution of 1 g and 2 kg of maximum capacity. Now, any downward thrust force from propulsion group at the end of main beam will create an upward force on the other end of tail beam. This setup is also used to find the external moment applied on the systems pitch dynamic.
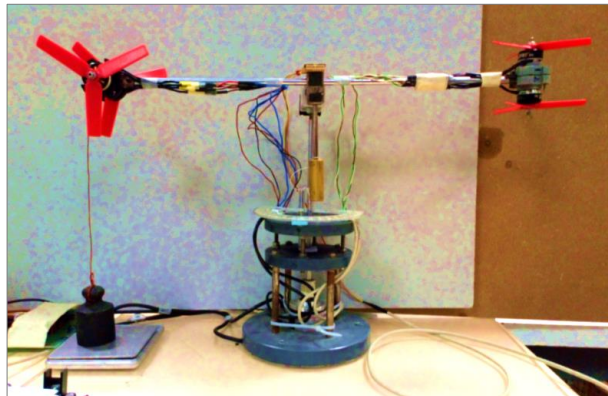
Figure 3.6. Static test setup for thrust measuring

The individual value of current drawn by propulsion system is recorded from the power supply unit screen, with corresponding input voltage value given in the form of PWM (%) as an input and ranges from 0-100. The angular speed of propeller is measured by using portable tachometer given in Figure 3.5.

Test Procedure

- All the components are connected accordingly as shown in Figure 3.6. The ESC is given a main power of 12 Volts from power supply with maximum current ranges from 0-30 Ampere.

- The 500 g weight is placed on the balance and the balance is set to zero reading. In this way, any upward left force on the 500 g weight makes an accurate negative force on the balance.

- For measuring the propeller angular speed, a small piece of white reflective paper was put on one of the propeller's blade. This reflective piece of paper then used by the tachometer to read the reflection of laser light generated by the tachometer.

- After a careful calibration of ESC, the test is started by incrementing the input voltage in the form of PWM ranges from 0-100 % with magnitude 2 increment. The corresponding output values of thrust force of propulsion group was recorded from balance in grams, the current drawn was notices and saved from power supply unit and the angular velocity of the propeller was measured using tachometer.

In Figure 3.7 below, thrust force is plotted against the quantity $\rho A(\omega R)^2$ and the slop represents the coefficient of thrust force C_T for the given propeller and motor combination. Table 3.2 show the recorded data for motors static thrust calculation.
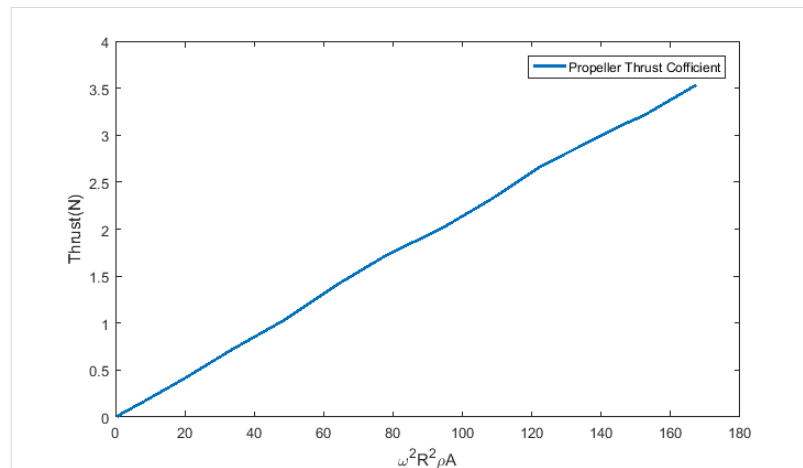
Figure 3.7. Thrust force vs $\rho A(\omega R)^2$

Table 3.2. Motor static thrust force and torque response against PWM

PWM Up motor (%)	PWM Down motor (%)	Force (N)	RPM	Current (A)	Torque (Nm)
51.5	48	-0.0039	806	0.12	0.00104
52	48	-0.0304	1478	0.19	0.00808
54	48	-0.1726	3520	0.52	0.04592
56	48	-0.4080	5360	1.11	0.10855
58	48	-0.7112	6953	1.98	0.18918
60	48	-1.0290	8397	2.96	0.27373
62	48	-1.4185	9671	4.28	0.37732
64	48	-1.7167	10640	5.48	0.45665
66	48	-2.0159	11717	6.95	0.53624
68	48	-2.3200	12556	8.65	0.61713
70	48	-2.6742	13365	10.4	0.71133
72	48	-3.1342	14653	12.5	0.83372
74	48	-3.3040	14870	14.48	0.87886
76 (saturation)	48	-3.5365	15608	15.78	0.94071
51.5	48	0.00072	650	0.12	0.00019
51.5	50	0.04141	2813	0.38	0.01101
51.5	52	0.15620	4547	0.782	0.04155
51.5	54	0.35963	6198	1.55	0.09566
51.5	56	0.58994	7556	2.372	0.15692
51.5	58	0.86820	8816	3.386	0.23094
51.5	60	1.18133	10062	4.665	0.31423
51.5	62	1.47122	11008	5.711	0.39134
51.5	64	1.81269	11964	7.292	0.48217
51.5	66	2.10548	12993	8.794	0.56005
51.5	68	2.39391	13824	10.19	0.63678
51.5	70	2.75718	14626	11.793	0.73341
51.5	72	3.09138	15123	11.941	0.82230
51.5	74 (saturation)	3.41614	15612	12.113	0.90869

3.7.1.2 Motor static test for torque calculation

In this test, the torque generated by the motor is analyzed in the similar method as explained in detail in the previous test for thrust calculation.

Figure 3.8. Static test setup for torque measuring

This test establishes a relation between input voltage in the form of PWM ranges from 0-100 % and the torque generate by the propulsion group, the current drawn in ampere

and the angular velocity of propeller in revolution per minute. In this test the motor is placed on a torque measuring device. This device can measure 3 axis torques that ranges from -10 to 10 Nm.

Test Procedure

All the necessary steps require for this test are same as mentioned in previous test for thrusts force calculation. The complete setup is shown in Figure 3.8 and the recorded data is given in Table 3.2. Figure 3.9 represent a plot of torque against $\rho A(\omega R)^2 R$ and the slope is the coefficient of torque C_Q.
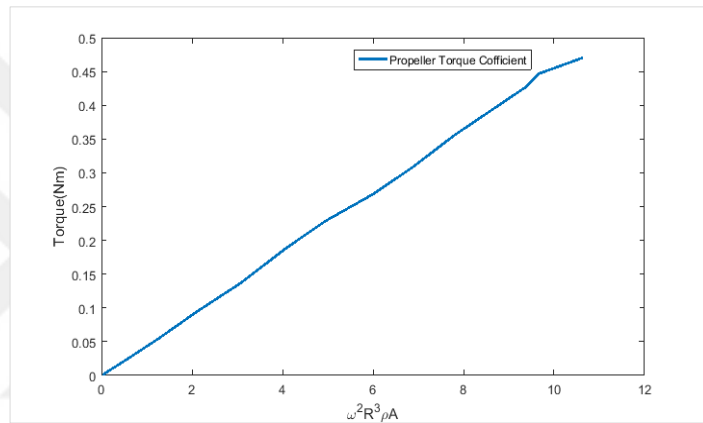
Figure 3.9. Torque vs $\rho A(\omega R)^2 R$
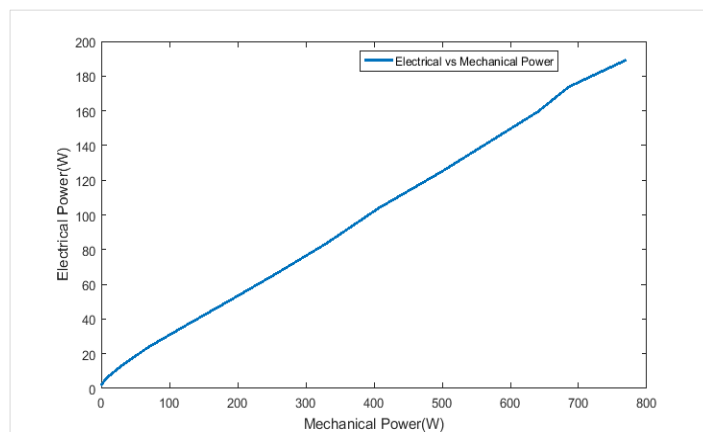
Figure 3.10. Electrical vs mechanical power

3.7.2. Motor performance test

In the test, current, torque and angular velocity of the motor were recorded as given in Table 3.2. Using this data, the efficiency of the motor-controller system, mechanical power output and electrical power input was analyzed.

The mechanical power output is computed from the angular velocity and torque and the electric power is computed from the voltage and the current using the data from Table 3.3. In Figure 3.10 electrical power is plotted against the mechanical power. The fitting, then yields the curve.

$$P_{electrical} = -0.00000705P_{mechanical}^2 + 0.248P_{mechanical} + 3.971 \tag{3.28}$$

The efficiency of the motor describes as the ratio of mechanical output power to the electrical input power given by

$$\eta_{motor+ESC} = \frac{\text{mechanical power output}}{\text{electrical power input}} \tag{3.29}$$

From equation (3.28) the efficiency of the motor and ESC, $\eta_{motor+ESC}$, becomes,

$$\eta_{motor+ESC} = \frac{P_{mechanical}}{-0.00000705P_{mechanical}^2 + 0.248P_{mechanical} + 3.971} \tag{3.30}$$
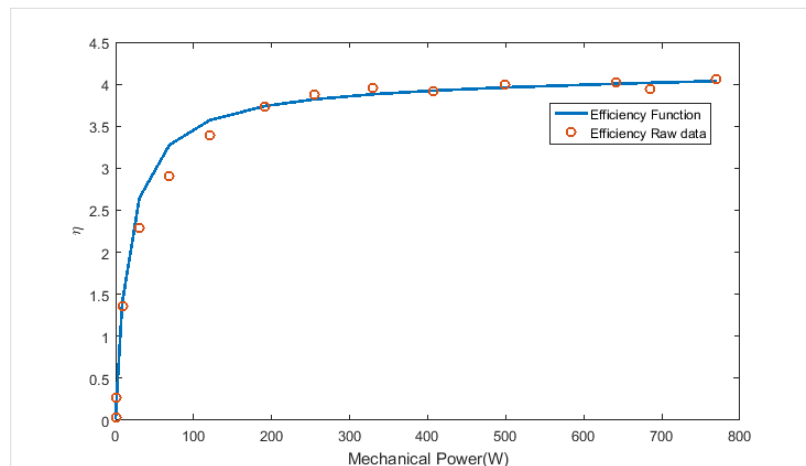
Figure 3.11. Efficiency vs mechanical power output

42

Table 3.3. Motor efficiency test data

Electrical Power (W)	Mechanical Power (W)	Efficiency fitted	Efficiency raw data
1.44	0.044125655	0.011084	0.030642816
2.28	0.62709345	0.152004	0.275040987
6.24	8.479133398	1.396359	1.35883548
13.32	30.51787268	2.646395	2.291131583
23.76	68.99321333	3.278092	2.90375477
35.52	120.5579287	3.570405	3.394085832
51.36	191.3973026	3.739816	3.726582994
65.76	254.8448216	3.81998	3.875377457
83.4	329.5523347	3.88013	3.951466842
103.8	406.4232914	3.923063	3.915445967
124.8	498.6444058	3.961241	3.995548123
159.6	640.7572793	4.005151	4.01476992
173.76	685.4553775	4.016721	3.94483988
189.36	770.1027283	4.036719	4.066871189

3.7.3. ESC performance test

Brushless DC motors need a controller to energize their coils according to the desired angular velocity. The control signal is sent via a PWM signal where the length of the high pulse determines the angular velocity of the motor. As it is a common practice in RC the high pulse is set to be between 1mS and 2mS. Thus 1mS meant 0% of throttle and 2mS meant 100% which represent 50% to 100% duty cycle values. To assess the behavior of the ESCs on their role of drivers of thrust generating devices, the throttle vs thrust is plotted in Figure 3.12. As it can be seen, the ESC shows a linear behavior near the operating point of feasible thrust demands which is 55% to 73% of the duty cycle.
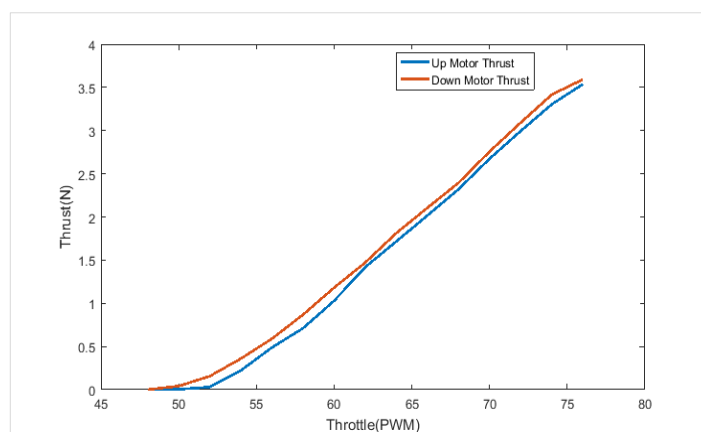
Figure 3.12. Motor thrust force vs throttle

To analyze the linearity of the controller, the angular speed in steady state has been plotted against the throttle position from 50% to 100% of duty cycle which is sent to

ESC. It can be seen in that around the nominal working point, 55% to 73% of throttle, it exhibits very linear behavior although in the edges, near 50% and 100%, the nonlinearities begin to arise.
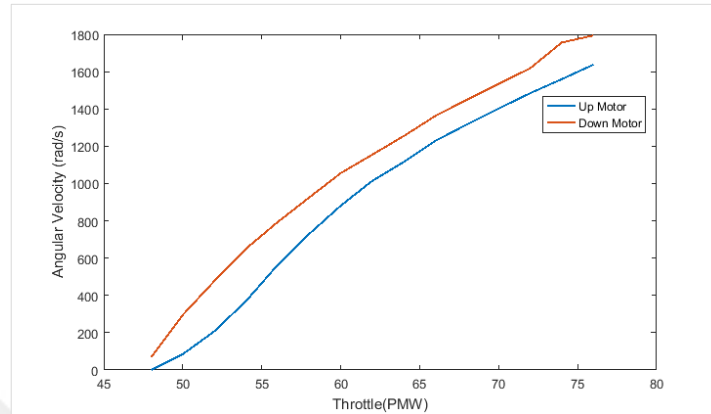
Figure 3.13. Motor speed vs throttle

3.8. Gravity Compensation

In robotic manipulators the desire reference point regulation is the main aim that can be solved using either PID control or by using the dynamic model information to design a gravity compensation function. These algorithms are mostly used in rigid body arms and to elastic joint or flexible arm robots. Nevertheless, the classical control algorithm like PID, need to perform a laborious job of gains tuning for achieving the most recommended performance in its constraint workplace. Moreover, there is no guarantee of global convergence using PID control law has proven yet for the robots having the elastic joint or flexible link. One of the well-known and simple solution for tracking the desire command signal is using only PD control law with constant value of gravity compensation and high position gain [59].

However, the requirement of gravity compensation for a system depends on the demand of the degrees of precision that the system can work satisfactorily. In the proposed DTRAS System, the tolerance that are allowed for the error to achieved the desire set point by pitch or yaw positon is between 0 to 1 degrees. Therefore, using the information of the dynamic model of the pitch motion, the gravity compensation function can be model for the pitch controller to generate the exact gravity compensating signal for the desire set point.

Table 3.4. Pitch angle against PWM

PWM Up motor (%)	PWM Down motor (%)	Pitch angle (degrees)
51.5	48	-9.3
52	48	-11.263
52.5	48	-13.52
53	48	-16.512
53.5	48	-20.633
54	48	-25.18
54.5	48	-28.913
55	48	-35.4912
55.5	48	-41.512
56	48	-48.512
56.5	48	-58.123
57	48	-67.912
51.5	48	-9.3
51.5	48.5	-7.721
51.5	49	-5.612
51.5	49.5	-2.4412
51.5	50	0.412
51.5	50.5	4.613
51.5	51	9.215
51.5	51.5	13.572
51.5	52	19.145
51.5	52.5	26.914
51.5	53	33.214
51.5	53.5	42.134
51.5	54	52.514
51.5	54.5	64.415
51.5	55	78.103

In the proposed system, the gravity compensation calculation take place online at a current position of the system by the nonlinear function which is estimated using the data recorded from experiment [60]. In this experiment, a set of input point to the system is fed and the corresponding position is recorded as shown in Table 3.4.

Referring to Figure 3.3 the gravity force moment acting on the system can be modeled that varies with pitch angle θ.

$$M_g = g\cos\theta \left[l_t \left(\frac{m_{tb}}{2} + m_{tm} \right) - l_m \left(\frac{m_{mb}}{2} + m_{mm} \right) \right] - l_{cb}g\sin\theta \left(\frac{m_{cb}}{2} + m_{cm} \right) \tag{3.31}$$

From Table 3.4 the up and down motors throttles (PWMs) with corresponding pitch angle response is then fitted to a third degree polynomial functions.

$$\theta = -0.1299T_u^3 + 19.6T_u^2 - 989.75T_u + 16716 \tag{3.32}$$

$$\theta = 0.1525T_d^3 - 21.892T_d^2 + 1052.2T_d - 16941 \qquad (3.33)$$

Where θ is the pitch angle, T_u is the up motor throttle and T_d is the down motor throttle in the form of PWM. Now in order to find the desire throttle value for a corresponding value of pitch angle position the above transfer functions need inversion. Using the data in Table 3.4 the inversion process is perform and the resulted fitted transfer function for throttles calculation for up and down motors are given by

$$T_u = -0.000020\theta^3 - 0.00380\theta^2 - 0.26340\theta + 49.475 \qquad (3.34)$$

$$T_d = 0.000010\theta^3 - 0.0020\theta^3 + 0.15020\theta + 49.797 \qquad (3.35)$$
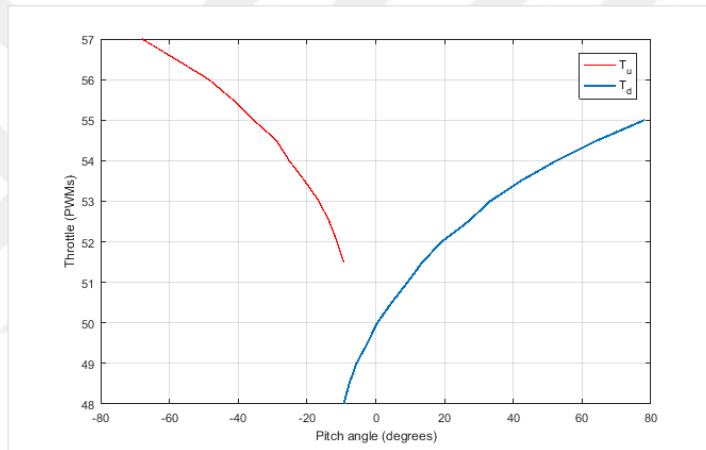
Figure 3.14. Pitch angle variation with PWM

3.9. Inertial Measurement Unit

Nowadays, all type of advanced aircrafts has a number of sensors which send the necessary information to the controller needed for maintaining the desire attitude and navigation. The IMU is one of that sensor device that contain a set of sensors needed for attitude and directing the aircrafts. The IMU consists of the following sensors:

- Gyroscope
- Accelerometer
- Magnetometer

All these sensors in three axes in a MEMS IMU sensor are calibrated according to the following model given below.

46

$$
\begin{bmatrix} y_x \\ y_y \\ y_z \end{bmatrix} = \begin{bmatrix} 1 & M_{xy} & M_{xz} \\ M_{yx} & 1 & M_{yz} \\ M_{zx} & M_{zy} & 1 \end{bmatrix} \begin{bmatrix} \dfrac{1}{S_x} & 0 & 0 \\ 0 & \dfrac{1}{S_y} & 0 \\ 0 & 0 & \dfrac{1}{S_z} \end{bmatrix} \begin{bmatrix} x_x \\ x_y \\ x_z \end{bmatrix} + \begin{bmatrix} b_x \\ b_y \\ b_z \end{bmatrix} + \begin{bmatrix} v_x \\ v_y \\ v_z \end{bmatrix} \tag{3.36}
$$

Where x_i is the sensor value along the ith axis, y_i is its calibrated output value, b_i is the bias value, v_i is the distributed Gaussian random error, S_i is the scaling factor and M_{ij} is the sensitivity parameter for the ith axis output to the jth axis input.

3.9.1. Gyroscope

This device measures the angular velocity about the three axis of the body frame of the IMU sensor if the frame of IMU body and gyroscope sensor is aligned. The sensor model is given by the following equation (3.37) below and the IMU calibrated gyro data is plotted in Figure 3.15.

$$
y_g = M_g S_g \omega + b_g + v_g \tag{3.37}
$$

Where $\omega = [p \ q \ r]^T$

3.9.2. Accelerometer

Accelerometer measure the actual acceleration of the body along the three axis of the sensor. This actual acceleration is the sum of linear acceleration which is time rate of linear velocity and the constant gravity acceleration g. Now, if a is the actual acceleration vector of the sensor body frame then the acceleration model is given by equation (3.38) and calibrated accelerometer data from IMU is plotted in Figure 3.15.

$$
y_a = M_a S_a a + b_a + v_a \tag{3.38}
$$

Where the components of the proper acceleration vector a is given by:

$$
\begin{bmatrix} a_x \\ a_y \\ a_z \end{bmatrix} = \begin{bmatrix} \dot{u} \\ \dot{v} \\ \dot{w} \end{bmatrix} + \begin{bmatrix} g\sin\theta \\ -g\cos\theta\sin\varphi \\ -g\co\theta s\cos\varphi \end{bmatrix} \tag{3.39}
$$

Where $\dot{u}$, $\dot{v}$ and $\dot{w}$ are the time rate of linear velocities vector components.

$$y_a = M_a S_a \left(\begin{bmatrix} \dot{u} \\ \dot{v} \\ \dot{w} \end{bmatrix} + \begin{bmatrix} g\sin\theta \\ -g\cos\theta\sin\varphi \\ -g\co\theta s\cos\varphi \end{bmatrix} \right) + b_a + v_a \qquad (3.40)$$

3.9.3. Magnetometer

Magnetometer sensor measures the level of magnetic field and its direction along the its axis. Using this value and the earth vector of magnetic field, the estimation of the aircraft attitude can be made. In according to the equation (3.41) the output of the magnetometer is given by:

$$y_m = M_m S_m m_b + b_m + v_m \qquad (3.41)$$

Where m_b is the magnetic field vector in the body frame, M_m and S_m are the misalignment factor and scaling matrices, b_m represents the sensor bias value and v_m is Gaussian random white noise value. Figure 3.15 shows the magnetometer data collected from IMU sensor with system off.
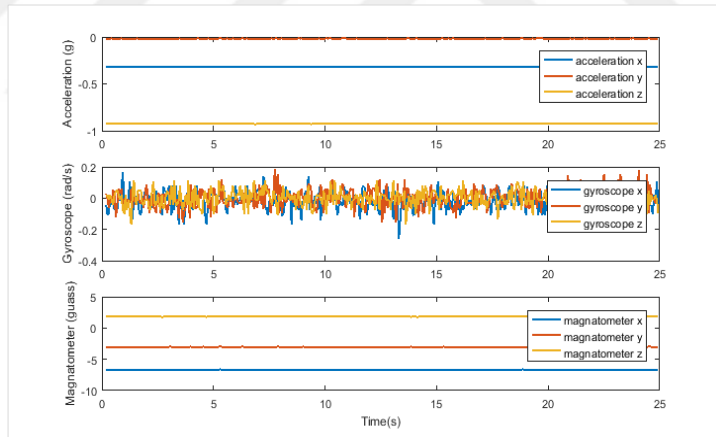
Figure 3.15. 3-axis IMU calibrated data

3.9.4. Calculating attitude information from IMU sensor

In this section two method are been used to calculate the attitude information from the IMU sensor. As explained above IMU sensor consist of 3-axis gyroscope, 3-axis accelerometer and 3-axis magnetometer. Using this data, complementary filter and Kalman filter are used to find the reliable information for orientation.

The IMU sampling rate of gyroscope, accelerometer and magnetometer is 110 samples per second and the corresponding specifications are given below in Table 3.5, Table 3.6 and Table 3.7 respectively.

Table 3.5. Gyroscope specifications

Dynamic range	+/- 2000 degrees/second
Sensitivity change vs temperature	+/- 0.04% /degree C
Bias change vs temperature	+/- 20 degrees/s from -40 C to +85 C
Total RMS noise	0.06 degrees/second rms
Rate noise density	0.005 degrees/second/root Hz
Cross-axis sensitivity	+/- 2% degrees/second
Non-linearity	0.2%
Mechanical frequency x-axis	33 kHz nominal
Mechanical frequency y-axis	30 kHz nominal
Mechanical frequency z-axis	27 kHz nominal
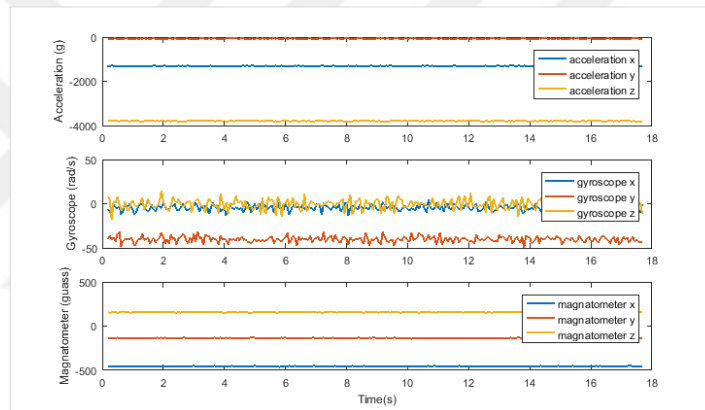
Figure 3.16. Raw data from gyroscope, accelerometer and magnetometer

Table 3.6. Accelerometer specifications

Sensitivity change vs temperature	+/- 0.02% / degrees C
Bias change vs temperature	+/- 0.75mg / degrees C
Bias change vs temperature	+/- 1.5mg / degrees C
Rate noise density	400 ug/root Hz
Dynamic Range	+/- 8g

Table 3.7. Magnetometer specifications

Initial scale factor tolerance	+/- 4%
Dynamic range	+/- 1200 uT
Initial bias tolerance	+/- 300 uT

The raw data of gyroscope, accelerometer and magnetometer are given in Figure 3.16 and the corresponding calibrated values are given in Figure 3.15. These data were

collected from the IMU sensor while the system was in home position i-e $\theta = \psi = 0$ degrees. In order to see the effect of the system components vibration, the system actuators were given a nominal voltage signal. The corresponding effect were then plotted as shown in Figure 3.17.

As can be seen in Figure 3.15, the accelerometer calibrated values for x and y axis are nearly zero while the z axis value is almost equal to 1g. this is because of the fact that at home position the gravity act only along the negative z-axis pointing downward. Despite the system been at rest position, gyroscope has a small fluctuating data values which is called a white noise. This noise is part of the gyroscope sensor value that become the source of drift in calculating the angular position. The quick response and accurate measurement of gyroscope with effect of angular motion make it reliable to calculate the angular position using time integration of its output value.
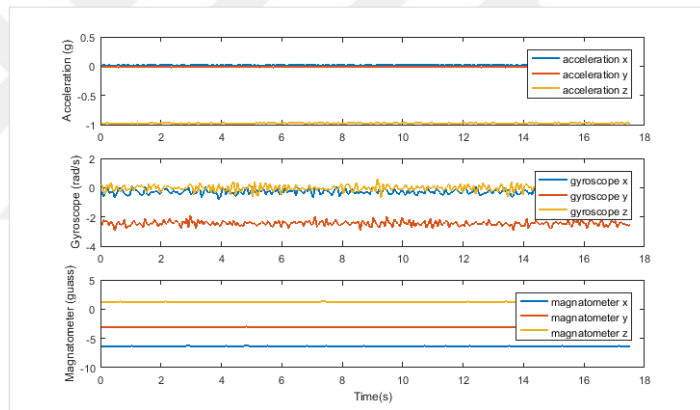
Figure 3.17. The effect of system components
vibration on IMU data

The trapezoidal integration method is used to find the angular position as given by equation (3.42)

$$\int_{k_i}^{k_{i+1}} f(x)dx = (k_{i+1}-k_i)f(k_i) + \frac{1}{2}(k_{i+1}-k_i)(f(k_{i+1})-f(k_i)) \qquad (3.42)$$

This resultant value from this relation drift from the real angular position value over time due to the noise from gyroscope output. This noise is integrated over time and accumulated to the real angular position. However, the integrated value has less noise as compare to the gyroscope output value. To avoid drifting, accelerometer is

considered to correct the drift from integration of gyroscope sensor output. But the problem with the accelerometer is that it is vulnerable to vibration as can be seen in Figure 3.17. Utilizing the technique of fusing the accelerometer, gyroscope and magnetometer output, a more reliable orientation information can be extracted. In this method first, the angular position is calculated separately from all the three sensors. These values are then fused by using various algorithm. In this report, two methods are used to fused the accelerometer, gyroscope and magnetometer data.

- Complementary Filter
- Kalman Filter

The complete sensor implementation algorithm is depicted in Figure 3.18.
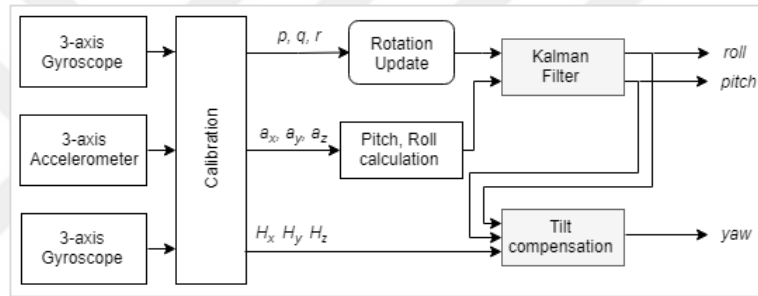
Figure 3.18. Sensor fusion algorithm

First, the gyroscope, accelerometer and magnetometer raw data are converted to a meaningful calibrated data and the required biases are applied to make the sensors output equal to zero. The calibrated information from accelerometer (gravity vector) are used to calculate the pitch and roll angle using the following equations and represented by θ_a and φ_a respectively.

$$\theta_a = a\sin(a_x) \tag{3.43}$$

$$\varphi_a = a\tan\left(\frac{a_y}{a_z}\right) \tag{3.44}$$

The pitch and roll angles from gyroscope sensor can be calculated by first finding the Euler rates using the following transformation matrix. This transformation matrix converts the body-angular rates to Euler rates. These Euler rates of pitch and roll angles are integrated using equation (3.46) and (3.47) and is given by θ_g and φ_g respectively.

$$\begin{bmatrix} \dot{\phi} \\ \dot{\theta} \\ \dot{\psi} \end{bmatrix} = \begin{bmatrix} 1 & \sin(\phi)\tan(\theta) & \cos(\phi)\tan(\theta) \\ 0 & \cos(\phi) & -\sin(\phi) \\ 0 & \dfrac{\sin(\phi)}{\cos(\theta)} & \dfrac{\cos(\phi)}{\cos(\theta)} \end{bmatrix} \begin{bmatrix} p \\ q \\ r \end{bmatrix} \tag{3.45}$$

$$\theta_g = \int_{t_i}^{t_{i+1}} \dot{\theta}(t)dt = (t_{i+1}-t_i)\dot{\theta}(t_i) + \frac{1}{2}(t_{i+1}-t_i)(\dot{\theta}(t_{i+1}) - \dot{\theta}(t_i)) \tag{3.46}$$

$$\phi_g = \int_{t_i}^{t_{i+1}} \dot{\phi}(t)dt = (t_{i+1}-t_i)\dot{\phi}(t_i) + \frac{1}{2}(t_{i+1}-t_i)(\dot{\phi}(t_{i+1}) - \dot{\phi}(t_i)) \tag{3.47}$$

The pitch angular position from accelerometer, θ_a and gyroscope, θ_g are fused together using complementary filter to get the resultant pitch angular position θ. Similarly, the roll angular position from gyroscope and accelerometer given by ϕ_a and ϕ_g are fused to get the resultant roll angle ϕ.

For calculating the yaw angle, ψ, a tilt compensation process is used in which the magnetometer calibrated data and resultant estimated data of roll and pitch are used. This angle is called the heading angle and is measured about the z-axis of inertial frame which is perpendicular to the earth surface. The Earth magnetic field is used with the help of 3-axis magnetometer from IMU sensor when it is kept parallel to the earth surface. However, in many cases the body of the aircraft varies its orientation that make the body of aircraft and IMU sensor out of the earth horizontal surface.

Therefore, the tilt compensation process is used to transfer the magnetometer data the earth horizontal surface using the estimated roll and pitch information to correct the tilt error and consequently provide the accurate heading information. If H_x, H_y and H_z are the calibrated three axis output of the magnetometer data then the heading , ψ, is given by the equation (3.50).

$$x_H = H_x\cos\theta + H_y\sin\theta\sin\phi + H_z\sin\theta\cos\phi \tag{3.48}$$

$$y_H = H_y\cos\phi + H_z\sin\phi \tag{3.49}$$

$$\psi = \text{atan2}\left(\frac{-y_H}{x_H}\right) \tag{3.50}$$

The complete attitude vector $q=[\theta \ \dot{\theta} \ \psi \ \dot{\psi}]$ of a nonlinear DTRAS system have noise accumulated by two main sources i-e System vibration and Sensor measurement noise. These noisy states from the system are then feed to the extended Kalman filter that uses the characteristics of the proposed system dynamic to estimate optimally the required attitude information for orientation.

3.10. Kalman Filter

In autonomous system theory and robotics control designing, in most of the cases the machine decides its behaviors on the bases of the estimated state variables values. These states variables can be any things like position, orientation presences of robot, other environmental entities and searching. In any case, sometimes their values are not known or it could not be measured directly. Therefore, to find the correct value there comes the need for an algorithm that help the system in guessing the most suitable appropriate value for the state variables. This requirement for estimation of states variables paved the way for new study so, called probabilistic robotics [58]. In this context one such filter algorithm devised by Rudolf Emil Kalman in 1960 [33,40]. This filter considers the discrete time linear dynamic system from the physical system and can be represented in a state space model given below.

$$x_k = F_k x_{k-1} + B_k u_{k-1} + w_k \tag{3.51}$$

$$E[w_k] = 0 \tag{3.52}$$

Where F_k is the state matrix, x_k is the state variables vector, B_k is the input matrix of the system, u_k is the vector for control variables and the w_k is the process noise of zero-mean with Gaussian distribution. This filter has also measurement model which is a linear function of states variables.

$$y_g = H_k x_k + v_k \tag{3.53}$$

$$E[v_k] = 0 \tag{3.54}$$

Where H_k is the measurement matrix and v_k is the measurement noise of same nature as w_k but uncorrelated. The estimation results of Kalman filter is optimal statistically. This estimation algorithm uses two steps named as Prediction and Update.

In prediction step, the system states are predicted using the system model information given in a state space form in below equation (3.55).

$$\hat{x}_k^- = F_{k-1}\hat{x}_{k-1} + B_{k-1}u_{k-1} \tag{3.55}$$

$$P_k^- = F_{k-1}P_{k-1} A_{k-1}^T + Q_{k-1} \tag{3.56}$$

Where $\hat{x}_k^-$ is the priori estimate performed using system model information and P_k^- is the priori covariance predicted at time k and Q_k is the covariance of the process noise from equation (3.56).

Now in update step, the priori estimate from the system model information is updated according to the measurement information. This operation is performed according to the given relation.

$$\hat{x} = \hat{x}_k^- + K_k(z_k - H_k\hat{x}_k^-) \tag{3.57}$$

$$P_k = (I - K_k H_k)P_k^- \tag{3.58}$$

Where $\hat{x}$ is the posteriori estimate, P_k is the posterior covariance error and K_k is the Kalman gain and updated using the following relation.

$$K_k = P_k^- H^T (H_k P_k^- P_k^T + R_k)^{-1} \tag{3.59}$$

Where R_k is the covariance of the measurement noise given by v_k from equation (3.53). In many practical uses of Kalman filter the covariance error matrices of process, Q and measurement R are time invariant. Analyzing equation (3.59) it can be notice that as the measurement error value R approaches zero, the gain K_k weights more the error between predicted and measurement values.

$$\lim_{R \to 0} K_k = H^{-1} \tag{3.60}$$

But, as the priori estimated error covariance P_k^- decreases, the Kalman gain K_k also decreases and weights the error between priori estimated value and measured value less.

$$\lim_{P_k^- \to 0} K_k = 0 \tag{3.61}$$

3.10.1. Kalman filter formulation for continuous time system

In case of continuous system model, the system model is a continuous differential equation.

$$\dot{x} = F(t)x(t) + B(t)u(t) + w(t) \tag{3.62}$$

With the measurement model is a continuous linear function of state vector.

$$z(t) = H(t)x(t) + v(t) \tag{3.63}$$

In continuous domain of Kalman filter the prediction and update steps are coupled, so the continuous Kalman filter comprises of the following two equations.

$$\dot{\hat{x}} = F(t)\hat{x}(t) + B(t)u(t) + K(t)[z(t) - H(t)\hat{x}(t)] \tag{3.64}$$

$$\dot{P}(t) = F(t)P(t) + P(t)F^T(t) - K(t)R(t)K^T + Q(t) \tag{3.65}$$

and the Kalman gain is given by

$$K(t) = P(t)H^T(t)R^{-1} \tag{3.66}$$

3.10.2. Extended Kalman filter

The main limitation that the Kalman filter encounter is that this filter need the dynamic system model and measurement model to be linear with states variables. However, there are many cases in which the system does not behave linearly and therefore, the simple Kalman filter cannot be used for good estimation.

The EKF is a non-linear modified form of the Kalman Filter to estimate the states of dynamic system which is nonlinear to some range nonlinearity. The EKF algorithm linearizes the nonlinear models at each interval of time into linear system. Equation

(3.67) and (3.68) represent the continuous and discrete nonlinear model of the physical system respectively.

$$\dot{x}(t)=f(x(t),u(t))+w(t) \tag{3.67}$$

$$x_k=f(x_{k-1},u_{k-1})+w_{k-1} \tag{3.68}$$

The nonlinear form of the measurement model is represented in below equations for continuous and discrete form.

$$z(t)=h\big(x(t)\big)+v(t) \tag{3.69}$$

$$z_k=h(x_k)+v_k \tag{3.70}$$

Similar to the simple Kalman filter, in the prediction step of extended Kalman filter the *apriori* state $\hat{x}_k^-$ and Kalman covariance P_k^- calculated, based on the input u and prior states data.

$$\hat{x}_k^-=f(x_{k-1},u_{k-1})+w_{k-1} \tag{3.71}$$

$$P_k^-=A_kP_{k-1}\,A_k^T+Q \tag{3.72}$$

Next, in the update step, based on the observation z, the Kalman *aposteriori* state $\hat{x}_k^-$, error covariance P_k^- and Kalman gain are calculated.

$$\hat{x}=\hat{x}_k^-+K_k(z_k-H_k\hat{x}_k^-) \tag{3.73}$$

$$P_k=(I-K_kH_k)P_k^- \tag{3.74}$$

$$K_k=P_k^-H_k^T(H_kP_k^-H_k^T+R)^{-1} \tag{3.75}$$

Now, the probability distribution of the states become non-Gaussian if the system states and measurement equation are nonlinear. Therefore, this non-Gaussian distribution have mean and covariance matrices that cannot fully describe the states. Therefore, the EKF uses the current estimated states around which state transition and measurement models are linearized using its Jacobians given by A_k and H_k. These

Jacobians are then use to update the covariance estimates using the algorithm of simple Kalman filter.

First using Euler's forward approximation of the system state transition equation (3.21) then expanding about equilibrium point (x^0, u^0) using Tylor series gives the Jacobean matrix (3.77) of the system. The same method used for calculating H.

$$x_1^{t+1} = x_1^t + x_2^t \, \delta t$$

$$x_2^{t+1} = x_2^t + \frac{\delta t}{J_\theta} \left((Al_t - Bl_m)g\cos x_1 + Cl_{cb}g\sin x_1 - U_\theta l_{mm} - Dx_4^2 \sin 2x_1 - x_2 k_p \right)$$

$$x_3^{t+1} = x_3^t + x_4^t \, \delta t$$
(3.76)

$$x_4^{t+1} = x_4^t + \frac{\delta t}{J_\psi(x_1)} \left(U_\psi l_{tm}\cos x_1 - x_4 k_y \right)$$

Where δt is the sampling time of the EKF loop. The Jacobean of the nonlinear function given in equation (3.72) is denoted by,

$$A_k = \left. \frac{\partial f^{t+1}}{\partial x^{t+1}} \right|_{x^0,u^0} = \begin{bmatrix} 1 & \delta t & 0 & 0 \\ \dfrac{\partial x_2^{t+1}}{\partial x_1} & \dfrac{\partial x_2^{t+1}}{\partial x_2} & 0 & 0 \\ 0 & 0 & 1 & \delta t \\ \dfrac{\partial x_4^{t+1}}{\partial x_1} & 0 & 0 & \dfrac{\partial x_4^{t+1}}{\partial x_4} \end{bmatrix}$$
(3.77)

Where the following relation hold for A_k,

$$\frac{\partial x_2^{t+1}}{\partial x_1}(x^0, u^0) = -Cl_c g \frac{\delta t}{J_\theta}$$
(3.78)

$$\frac{\partial x_2^{t+1}}{\partial x_2}(x^0, u^0) = 1 - \frac{k_\theta}{J_\theta}\delta t$$
(3.79)

$$\frac{\partial x_4^{t+1}}{\partial x_1}(x^0, u^0) = -\frac{U_\psi^0}{J_\psi(\theta)}\delta t$$
(3.80)

$$\frac{\partial x_4^{t+1}}{\partial x_4}(x^0, u^0) = 1 - \frac{k_\psi}{J_\psi(\theta)}\delta t \tag{3.81}$$

$$H = I_{4x4} \tag{3.82}$$

The covariance matrices for the process and measurement noise are given by,

$$Q = \begin{bmatrix} 0.0001 & 0 & 0 & 0 \\ 0 & 0.0001 & 0 & 0 \\ 0 & 0 & 0.0001 & 0 \\ 0 & 0 & 0 & 0.0001 \end{bmatrix}$$
$$R = \begin{bmatrix} 0.02 & 0 & 0 & 0 \\ 0 & 0.5 & 0 & 0 \\ 0 & 0 & 0.03 & 0 \\ 0 & 0 & 0 & 0.6 \end{bmatrix} \tag{3.83}$$

respectively.

3.10.3. Linear and extended Kalman filter output verification

Validation of sensor data is an important process needed during data extraction and acquisition from the processing modules of the multi sensor devises like IMU. Each sensor in IMU, provide the measure data, which is normally a one dimensional time series. These kind of all the data measurement from the sensors are called raw data that need be validated before using it to make certain the accuracy and reliability of the resultant values which is then called processed data.

Therefore, to get the most reliable and accurate information from such module, needed for activating various actuator of system, this processes of validation need to consider external environmental conditions. This process of data validation is applied to data acquisition step and also to the data processing step. This increases the level of confidence of the system when the output of the system has great importance as desired such as in areas of medical diagnosis. DTRAS system uses IMU sensor module that consists of accelerometer, gyroscope, magnetometer, GPS unit, barometer and temperature sensor. In order to get the reliable system states from the set of sensors from the IMU unit, data processing and data fusion algorithms are applied. The DTRAS system require the accelerometer, gyroscope and magnetometer data to be processed for measuring its reliable dynamic states.
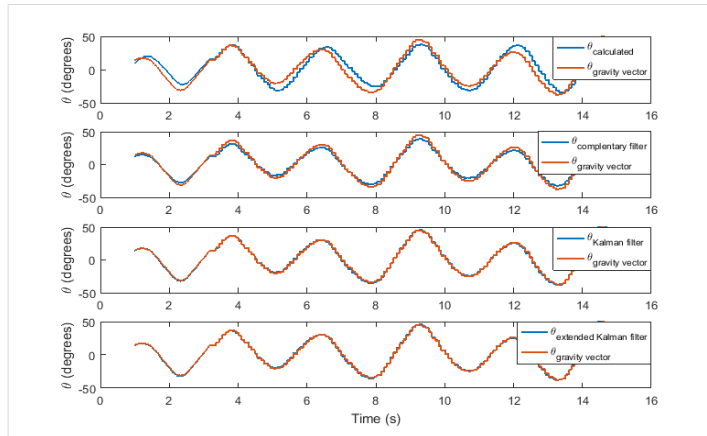
Figure 3.19. Pitch angle estimation using EKF, KF and complementary filters.

Therefore, in first step fusion algorithm is applied to fuse the data from the accelerometer, gyroscope and magnetometer sensors using Linear Kalman Filter as explained in section 3.9.4 and the results are given in Figure 3.19. The estimated results from using complementary filter, linear filter and extended Kalman filter are compared with absolute value of pitch angle calculated from accelerometers gravity vector using equation (3.43).
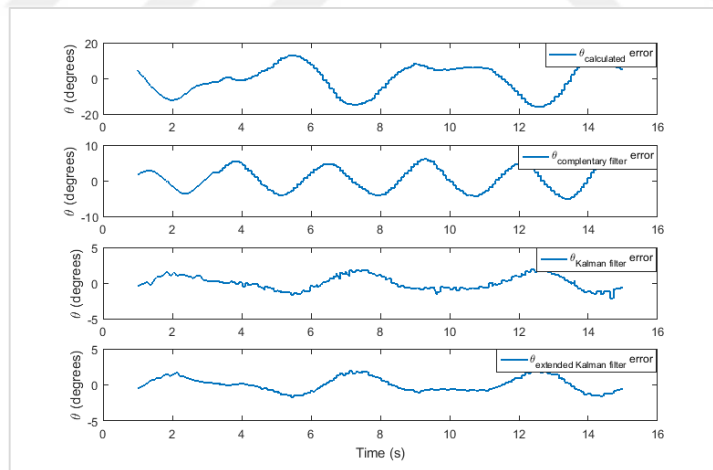
Figure 3.20. Filters estimation errors

In the second step EKF is designed using the dynamics of DTRAS system for eliminating the noises maintained after fusion process. The fusion and estimation processes using Linear and EKF is already explained in section 3.9.4 and 3.10.2 respectively.

59
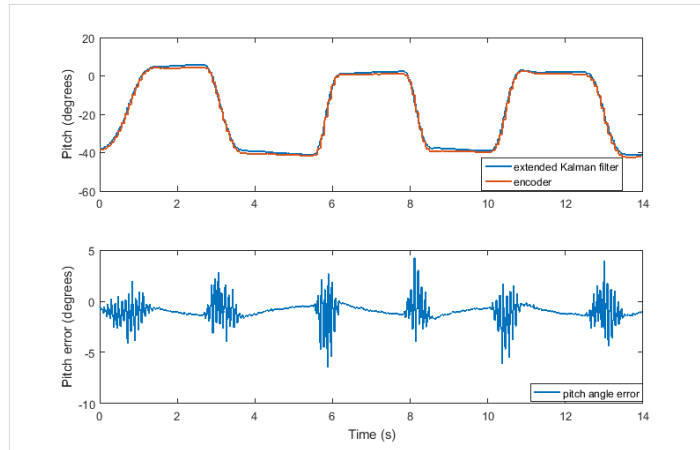
Figure 3.21. Pitch angle output of EKF and encoder.

The resulted estimated states from EKF is then compare with already calibrated encoder data as shown in Figure 3.21 and Figure 3.22 which shows the validness of the IMU measured data.
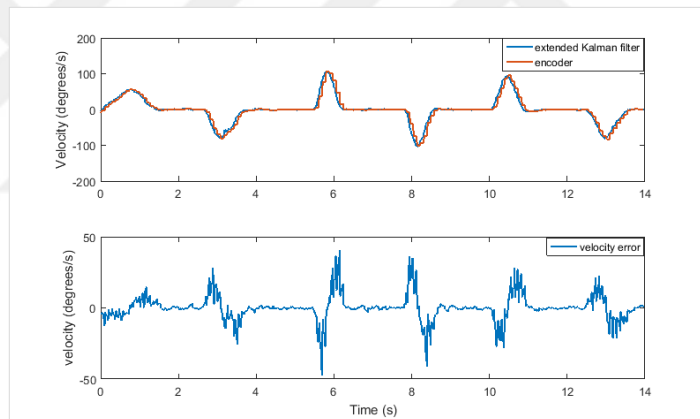
Figure 3.22. Pitch velocity output of EKF and encoder

3.10.4. Angular acceleration estimation

As explained in section 3.3 the angular acceleration calculated by time derivative of the angular velocities are noisy. For removing this noise, a modified form of moving average filter is designed. The estimation algorithm of this filter is elaborated as follow. Acceleration, rate of change of velocity, can be computed in the microprocessor using equation (3.84). Where $\partial\dot{\theta}$ is the change in angular velocity in a time duration ∂t. This relation for the calculated acceleration is plotted in Figure 3.23, represented with blue color curve.

60

$$\ddot{\theta}=\frac{\partial \dot{\theta}}{\partial t} \tag{3.84}$$

As can be seen the calculated acceleration curve has noise with signal to noise ratio (SNR) equal to 8.8906 db, which is calculated using the relation given by (3.85).

$$SNR=20 \log_{10}\left(\frac{X_s}{N_s}\right) \tag{3.85}$$

Where X_s, is the signal and N_s, is the noise of the signal.

The second order infinite impulse response filter (IIR) mechanism is used to smooth the noisy acceleration signals. This mechanism of IIR filter is given in relation (3.86).

$$F[n]= \frac{1}{2}\sum_0^k b_k\, x[n\text{-}k]+ \frac{1}{2}\sum_0^k a_k\, y[n\text{-}k]+e \tag{3.86}$$

$$e= \frac{1}{2}\left(\sum_0^k a_k\, y[n\text{-}2k+5]\text{-}\sum_0^k b_k\, x[n\text{-}2k+5]\right) \tag{3.87}$$

Where, e is the error signal, represents the difference between successive samples values. The resultant, filter estimation gives an approximated signal with reduced noise as shown in Figure 3.23 which is represented by a brown color curve.
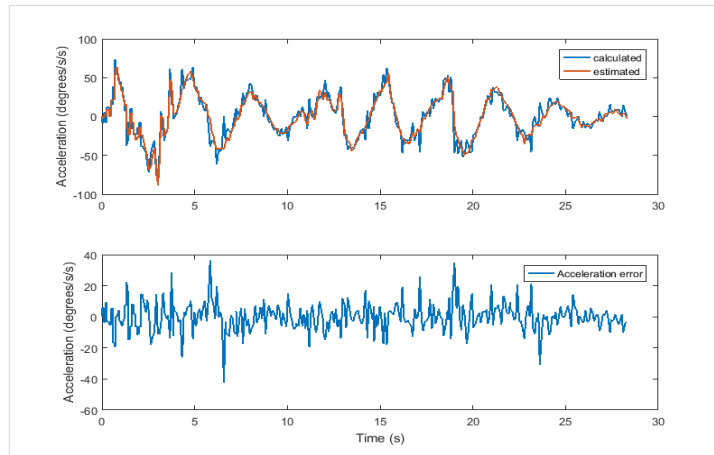
Figure 3.23. Acceleration estimation using infinite impuls
response (IIR) filter.

4. CONTROL DESIGN

This chapter gives an explanation about the development of the control strategies for Double Twin Rotor Aerodynamic System (DTRAS). The main general architecture for the control designs is given in Figure 4.1. The control system for DTRAS comprises of two main constituents, the control allocation part and the control law scheme. The control law guides the system by calculating the control signals based on the desire position trajectory and the system states information from the IMU sensor. This control signals are then feed to the control allocator unit where it is distributed to all the four actuators.
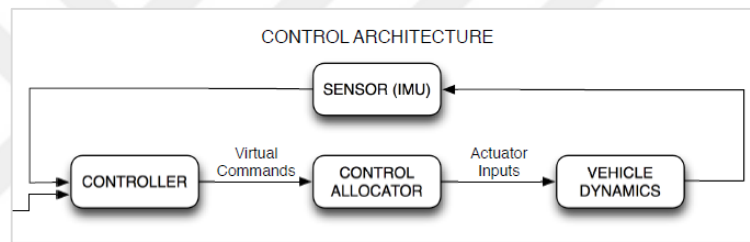
Figure 4.1. General Structure of the control design scheme

The development of control allocator is described in first section of this chapter. A short introduction is given about the concept of control allocation in the context of proposed system. Second, the selection of information for the control allocation scheme is discussed. Finally, the development of the gain matrix is introduced that shape the control signals for actuators to obtain the required actuation. The designed trajectory generated in the controller unit is fed to the control law along with the IMU states that are estimated using EKF. As the system is overactuated, uses two actuators for controlling the pitch or yaw motion, the control law uses two separate controllers that make switching according to the position state. This control law is based on the cascaded full-state feedback of position, velocity and acceleration of the system. These gains are same for yaw controllers and different for pitch controllers. There is no force other than the friction force and propulsive force of the motors that are positioned at equal distance from the yaw axis and parallel/symmetrical to/in the yaw plan. The difference in gains of pitch controllers are due to the fact that gravity cause disturbance

in pitch motions. These gains are found independently using trial based approach. For controlling Pitch motion of the system, the gravity must be compensated as there is no integral action used. Gravity compensation is performed, by analyzing the system dynamic model and implemented using the position feedback of the system as an input to the compensation function. In order to calculate the gains for the controllers of pitch and yaw motions, simple model is constructed and a close loop control analysis are performed.

The second strategy implemented is based on the PID control theory. This control strategy is designed in a similar method as cascaded full-state feedback algorithm. Two separate PID controllers are used each for two actuators of the pitch motion. However, PID controllers do not use the gravity compensation function as it uses integral action for keeping the system in desire position when the PD action is zero at reference point. The results of these two algorithm are compared which shows that the cascaded full-state feedback has good performance.

4.1. Cascaded Full State Feedback Control

As the name suggest, the control algorithm applied to the DRTAS system uses the position, velocity and acceleration as feedback information to control the system position. As explained before in Introduction chapter, the DTRAS system is an overactuted system uses two actuators for controlling one DOF.

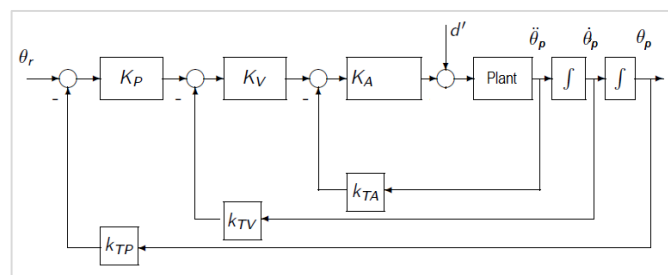Figure 4.2. CFSF controller without integrator

Therefore, a control allocator is needed to engage the actuators with proper distributed signals. In section 1.5, Figure 1.4 depicts the scheme used for the DTRAS system that uses the feedback information to distribute the control signal U_c using a simple gains matrix. This matrix then generates two signals, V_u and V_d correspond to up and down motors.

In the DTRAS system, for pitch position control two motors, up and down are used and in a similar way for yaw position control two motors left and right motors are used. The down motor provides upward thrust while the up motor gives downward thrust. This combination of thrust generation gives the idea of damper that restrict the system to a reference point by engaging both motors using the control allocator scheme.

The two pitch motors are controlled by two separate controllers that worked against each other in such a way to attain a local reference point by switching the main control signal to the require motor. This switching decision is performed according to the measured current position, velocity and acceleration of the DTRAS system. The generalized single controller for a single motor algorithm is depicted in Figure 4.2. The parameters are described in below.

Table 4.1. Controller parameters

Parameters	Descriptions
K_P	Position controller gain
K_V	Velocity controller gain
K_A	Acceleration controller gain
k_{TP}	Position feedback scaling
k_{TV}	Velocity feedback scaling
k_{TA}	Acceleration feedback scaling
d'	External disturbance

The virtual command signal u_c is the controller signal calculated using the fullstate feedback information and is given by

$$u_c = \left[\left\{ (\theta_r - \theta_P) K_P - \dot{\theta}_P \right\} K_V - \ddot{\theta}_P \right] K_A \tag{4.1}$$

The generalized controller represented by equation (4.88) is separately designed to generate the PWMs for up and down motors of the pitch motors. The complete flow chart that describes the function of up and down controllers and the control allocator for the pitch motion is given in Figure 4.3.
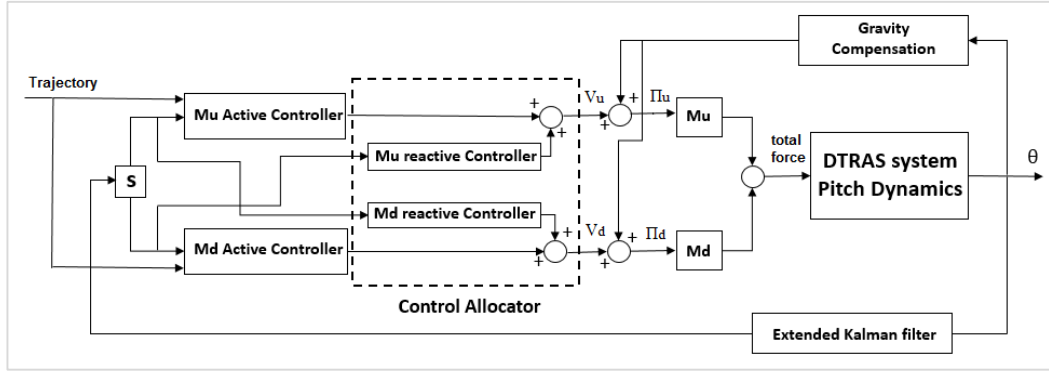
Figure 4.3. Distributed CFSF control for DTRAS system

4.1.1. Control allocator design

As explained before the thrusts generated by the pitch motors are acting against each other based on the position error. If the position in positive, the down motor is activated to create upward thrust and the up motor becomes active for downward thrust when the error is negative. This switching of activating pitch controllers based on the sign of position error creates chattering of high amplitude. This is due to the fact that only one controller (motor) is active at a time for one sign (positive or negative) of position error.

To avoid this high amplitude chattering, the control allocator is design that uses reactive controller to engage the non-active motor at all-time. Thus, the system pitch motors are controlled by active and reactive controllers at a time. This reactive controller, u_r given by equation (4.2), in the control allocator uses the position and velocity information to calculate the require actuating signal (PWM) for the motor that creates opposite thrust. This require value opposite thrust is determined by parameters K_P and K_V. Thus, restricting the system to overshoot and avoid the chattering to a minimum amplitude.

$$u_r=\{(\theta_r-\theta_P)K_P-\dot{\theta}_P\}K_V \tag{4.2}$$

In Figure 4.3, the control allocator adds the Down reactive control component, u_{drc} to the Down active controller u_{dac}. The resultant control signal is added with the gravity compensation component, $\Gamma(\theta)$ as a disturbance to give the actual control signal, Π_D for down motor and is given by following equation (4.3).

$$\Pi_D = \Gamma(\theta) + u_{dac} + u_{drc} \tag{4.3}$$

Where $\Gamma(\theta)$ is the gravity compensation function found by inversion of the pitch dynamics of the DTRAS system described in section 3.8. The active and reactive control components, u_{dac} and u_{drc} respectively are given by following relations.

$$u_{dac} = \frac{1}{2}\{sgn(\theta_r - \theta_P) + 1\}[\{(\theta_r - \theta_P)K_P - \dot\theta_P\}K_V - \ddot\theta_P]K_A \tag{4.4}$$

$$u_{drc} = -\frac{1}{4}\{sgn(\theta_p - \theta_r) + 1\}\{sgn(\dot\theta) - 1\}\{(\theta_r - \theta_P)K_P - \dot\theta_P\}K_V \tag{4.5}$$

Where θ_p and θ_r are the current pitch angle and the reference angle respectively. Similarly, for the Up active and reactive controller the following relation hold.

$$u_{uac} = \frac{1}{2}\{sgn(\theta_p - \theta_r) + 1\}[\{(\theta_p - \theta_r)K_P + \dot\theta_P\}K_V + \ddot\theta_P]K_A \tag{4.6}$$

$$u_{urc} = \frac{1}{4}\{sgn(\theta_r - \theta_p) + 1\}\{sgn(\dot\theta) + 1\}\{(\theta_r - \theta_P)K_P + \dot\theta_P\}K_V \tag{4.7}$$

The resultant actual control signal, Π_U for the up motor is given by the following relation.

$$\Pi_U = \Gamma(\theta) + u_{uac} + u_{urc} \tag{4.8}$$

In designing control yaw for yaw motion of the DTRAS system, there is no gravity moment involve therefore, the only moments responsible for yaw motion about z-axis are created by the thrust forces of the left and right motors. Therefore, the actual control signals of the left and right motors, Π_L and Π_R respectively are given by the following relations.

$$\Pi_L = u_{lac} + u_{lrc} \tag{4.9}$$

$$\Pi_R = u_{rac} + u_{rrc} \tag{4.10}$$

Where u_{rac} and u_{rrc} are the right active and reactive control signal respectively and are given by the following relations.

$$u_{rac}= \frac{1}{2}\left\{sgn\left(\psi_y-\psi_r\right)+1\right\}\left[\left\{\left(\psi_y-\psi_r\right)K_P+\dot{\psi}_y\right\}K_V+\ddot{\psi}_y\right]K_A \qquad (4.11)$$

$$u_{rrc}= \frac{1}{4}\left\{sgn\left(\psi_r-\psi_y\right)+1\right\}\{sgn(\dot{\psi})+1\}\left\{\left(\psi_r-\psi_y\right)K_P+\dot{\psi}_P\right\}K_V \qquad (4.12)$$

Where ψ_r and ψ_y are the reference yaw angle and current yaw angle respectively. Similarly, the left active and reactive controllers respectively are given u_{lac} and u_{lrc} which hold the following relations.

$$u_{lac}= \frac{1}{2}\left\{sgn\left(\psi_r-\psi_y\right)+1\right\}\left[\left\{\left(\psi_r-\psi_y\right)K_P-\dot{\psi}_y\right\}K_V-\ddot{\psi}_y\right]K_A \qquad (4.13)$$

$$u_{lrc}= -\frac{1}{4}\left\{sgn\left(\psi_y-\psi_r\right)+1\right\}\{sgn(\dot{\psi})-1\}\left\{\left(\psi_r-\psi_y\right)K_P-\dot{\psi}_y\right\}K_V \qquad (4.884)$$

4.2. PID Control

In classical control theory, PID (Proportional Integrator Derivative) controller is the easiest control strategy to implement for linear and non-linear systems. In designing PID controller for the DTRAS system, the gravity compensation factor is not used as the integral action fulfills the requirement to eliminate the steady state error. The PID control strategy applied on the DTRAS system is shown in Figure 4.4.

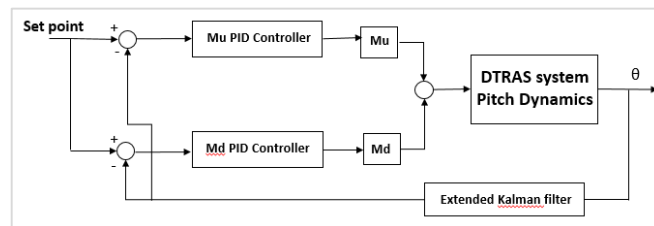Figure 4.4. PID control strategy for DTRAS system

The same strategy of designing two separate PID controllers for up and down motors are applied as in case of CFSF controller in section 4.1. The generalized PID control law is represented by the following relation.

$$u_c=f(e)K_P+\int f(e)dt+f(\dot{e})dt \qquad (4.15)$$

The down and up PID controller signals are given by the following relations.

$$\Pi_D = (\theta_r - \theta_P)K_P + K_I \int (\theta_r - \theta_P)dt + \dot{\theta}_P dt \tag{4.16}$$

$$\Pi_U = (\theta_p - \theta_r)K_P + K_I \int (\theta_p - \theta_r)dt - \dot{\theta}_P dt \tag{4.17}$$

The PID controllers are following the same concept as the follow.

In similar manner like CFSF controller, the PID controllers of the up and down motors are acting in opposite direction to produce opposite thrusts forces. As a result, both controller acting against each other to attain a local reference point by minimizing their error positions.

4.3. Fuzzy Logic Control

The idea of implementing the fuzzy logic control to various applications originates by analyzing the modeling of the system with uncertainties in the system behavior. This vagueness arises from the complex nature of the system itself. The method of approaching this kind of difficult problem is to diminish the complexity by developing variables with increased uncertainty [61]. These behaviors are studied through a vague and ambiguous fuzzy sets and rules. In a fuzzy system approach, the systems variables that act as linguistic variables and their values are also linguistic in terms that is modeled as a fuzzy set. By forming the rules based on these set of variables a general methodology can be develop to control these nonlinear systems. Therefore, the problem presented in this thesis report that shows highly non-linear behavior and classical control methods are toughest to apply, these techniques are very beneficial and easy to use [62].

To implement this control scheme to the propose DTRAS system, the fuzzy logic algorithm must be adjusted to the input and output variables that represents the sensors and actuators of DTRAS system. The generalized scheme is shown in Figure 4.5 described in [62].
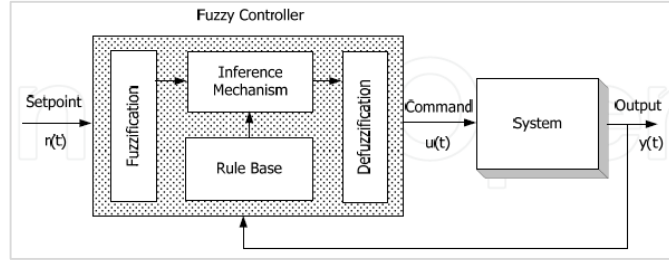
Figure 4.5. Generalized fuzzy logic controller scheme

As the DTRAS system explained earlier in chapter 3, it has four input, two each for pitch motors and yaw motors and two outputs each for pitch and yaw angel. The IMU sensor outputs which is the estimated position, velocity and acceleration for each DOF of DTRAS system can be used as feedback information in close loop control. However, in this control algorithm, position and velocity are considered as an inputs for fuzzy logic controller. As the DTRAS system has two DOF each controlled by 2 motors, therefore, two separate FLCs are designed each controlling the PWM of up or down motor for pitch motion control. Similarly, the same process is performed for the yaw motion control. In implementing the fuzzy logic controller, the algorithm requires the values given by the sensor must therefore be converted into the fuzzy values. These sensor values are the variables in the rule base that act as inputs for the fuzzy controller.

4.3.1. Input and output of fuzzy controller

Assuming the expert system in close loop system of the DTRAS system that regulate the control signal by making use of the base rule and the information it receives. This information act as inputs that FLC takes for the decision making process. For the DTRAS system, the FLC takes the error in position and the rate of variation in this position error as two inputs to carry out the decision based on the results obtained from equation (4.18) and (4.19).

$$e(t)=r(t)-y(t) \tag{4.18}$$

$$\dot{e}(t)=f(e,t) \tag{4.19}$$

Where, the error $e(t)$ is defined as the difference between the desired, $r(t)$ and measured, $y(t)$ position of DTRAS system.

69

The output that need to be control by FLCs of pitch motion is the PWMs of pitch motors. FLC UP and FLC DOWN control the PWMs of the up and down motors respectively. It is interesting to note that the same input information is given to the up and down FLCs. It is due to the fact that the signs of the input information are inverted for the FLC DOWN with respect to FLC UP and with different base rules because of the gravity moment. The complete FLC algorithm for the DTRAS system is depicted in Figure 4.6.
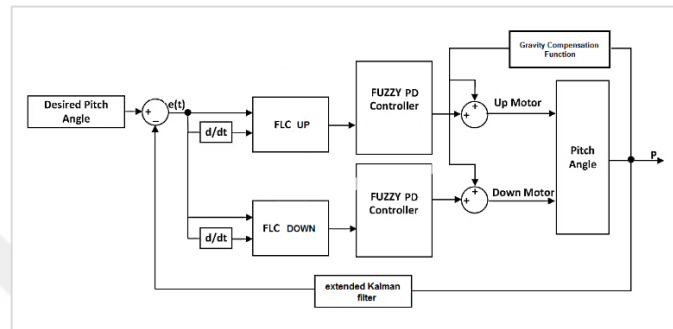
Figure 4.6. FLC scheme for controlling pitch motion

The linguistic description in the process of FLC design are the variables that describe the time varying inputs and outputs of the FLC. Therefore, for the DTRAS system of pitch motion, the following set of inputs and outputs variable are linguistically described and is given in Table 4.2.

- Position error represented by e(t)
- Variation in position error is represented by $\dot{e}(t)$
- Duty cycle (PWM) represented by DC

Table 4.2. Linguistic description for input output variables

Symbol	Definition	Function
VNL, VPL	Very Negative Large, Very Positive Large	Input
NL, PL	Negative Large, Positive Large	Input
NM, PM	Negative Medium, Positive Medium	Input
NS, PS	Negative Small, Positive Small	Input
ZE	Zero	Input
QT	Quiet	Output
VS	Very Slow	Output
S	Slow	Output
M	Medium	Output
F	Fast	Output
VF	Very Fast	Output

Now for controlling the pitch angle, the above position error, variation in position error, and the duty cycle (PWM) of the pitch motors that are responsible for controlling

the pitch dynamics of the DTRAS system takes the following states in Figure 4.7 in terms of its descriptors shown in Table 4.2.
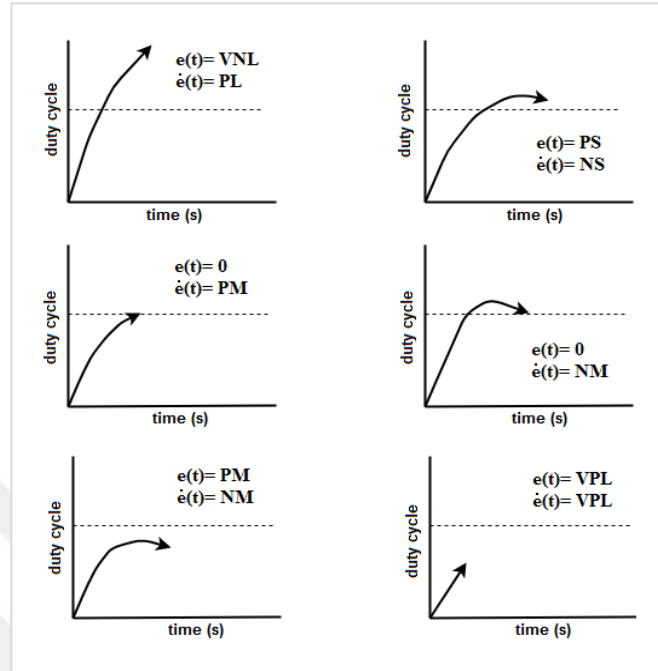
Figure 4.7. DTRAS pitch position in various states

The rule base developed by expert's knowledge for concluding the duty cycle value of the pitch motors and yaw motors for a particular states of $e(t)$ and $\dot{e}(t)$ are mentioned in Table 4.3 and Table 4.4 respectively.

Table 4.3. FLC rules for pitch motors.

$e\backslash\dot{e}$	VNL	NL	NM	NS	ZE	PS	PM	PL	VPL
VNL	F	M	S	QT	M	VS	S	S	QT
NL	M	S	VS	VS	S	S	S	S	QT
NM	F	M	S	VS	VS	VS	S	M	S
NS	M	M	S	VS	QT	VS	S	S	M
ZE	S	VS	QT	QT	QT	QT	VS	S	S
PS	F	M	S	VS	QT	VS	S	S	S
PM	F	M	S	S	VS	S	S	M	S
PL	VF	F	M	S	S	VS	S	M	M
VPL	VF	F	M	M	M	S	S	M	M

Table 4.4. FLC rules for yaw motors.

$e\backslash\dot{e}$	VNL	NL	NM	NS	ZE	PS	PM	PL	VPL
VNL	M	S	VS	QT	M	M	M	F	VF
NL	M	S	VS	VS	S	S	S	F	F
NM	M	S	S	VS	VS	VS	S	M	F
NS	S	M	S	VS	QT	VS	S	S	M
ZE	S	VS	QT	QT	QT	QT	VS	S	S
PS	S	VS	S	VS	QT	VS	S	M	M
PM	S	M	S	S	VS	S	S	M	M
PL	QT	S	M	VS	S	VS	M	M	M
VPL	QT	S	S	M	M	M	M	M	F

4.3.2. Fuzzy quantification of information

Using the expert knowledge of the DTRAS system that are developed in Table 4.3, for the pitch motors and Table 4.4, for the yaw motors, quantification of the input and output linguistic variables is performed using the membership functions.

For DTRAS system, the input ($e(t)$ and $\dot{e}(t)$) and the output (duty cycle) of the FLCs of pitch and yaw controllers are partitioned groups based on the Mamdani type membership function. Both the inputs, $e(t)$ and $\dot{e}(t)$ consists of nine overlapped groups with a range [-90,90] and distribution is shown in Figure 4.8 and Figure 4.9 respectively. The output, on the other hand, consists of six groups of overlapped distribution with range [0,100] as shown in Figure 4.10.

When $e(t)=\dot{e}(t)= 0$, it can be inferred from the rule base that the system is at the desired position and the system is at steady state. Therefore, the duty cycle outputs from the pitch FLCs must be set to zero with only the gravity compensation provide the desire values of PWMs to the pitch motors in order to keep the system at reference position.
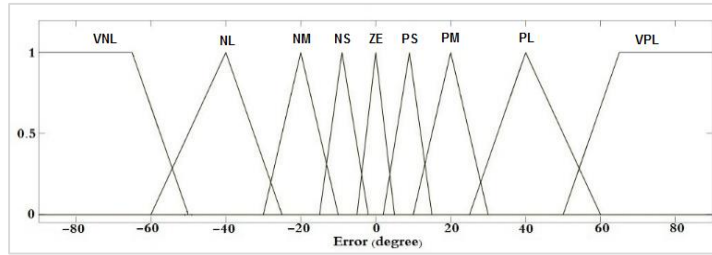
Figure 4.8. FLC input partition for pitch position error
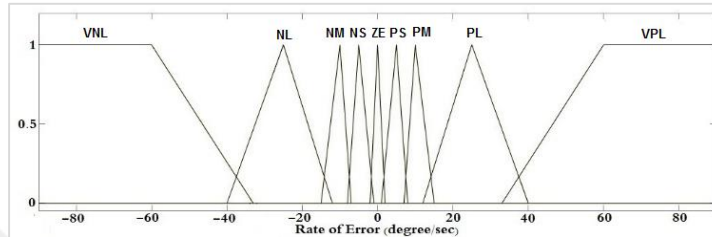
Figure 4.9. FLC input partition for pitch error variation
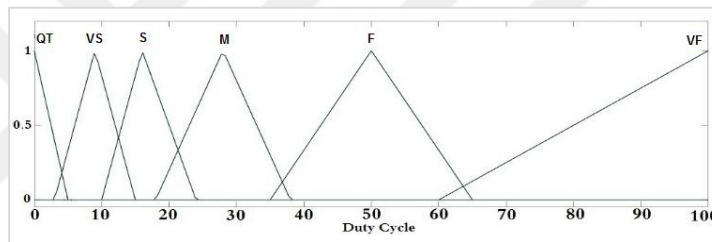
Figure 4.10. FLC output partition for duty cycle

Another example, in which the DTRAS states produce the $e(t)$= NL and the $\dot{e}(t)$= PL; this states suggests that the system has cross the reference point and keep moving with increasing error. The inference mechanism deduces the output of the up motor is F and down motor is slow.
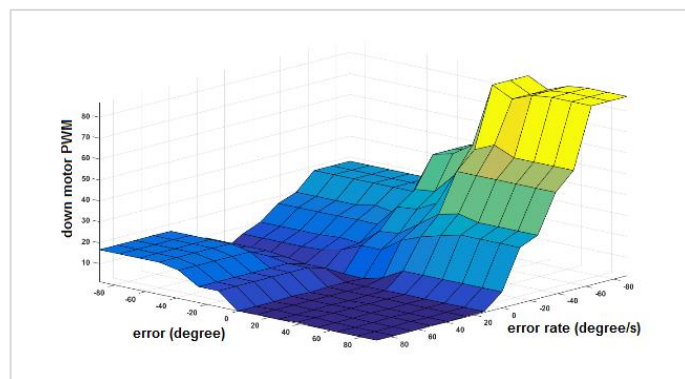
Figure 4.11. Down motor FLC control surface
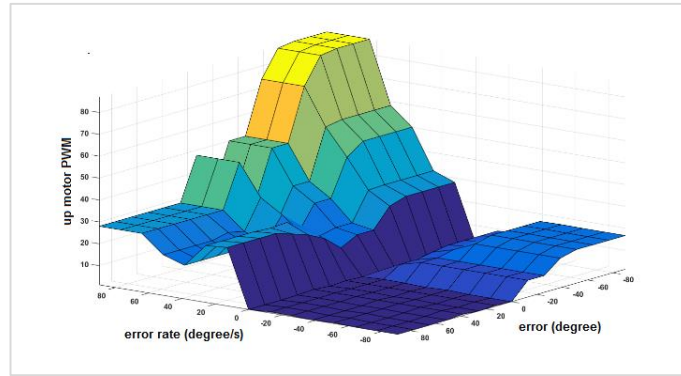
Figure 4.12. Up motor FLC control surface

Figure 4.11 and Figure 4.12 show respectively the down and up motor control signal that varies along the control surface according to the position error and error rate states of the pitch motion of the DTRAS system.

In Figure 4.11, it is clearly understandable that if the error rate is negatively high (moving downward) and the position error is increasing positively then the control action of the down motor would be such that it gives opposite upward thrust, providing high PWM value (control signal).

In the similar way the up motor would get the high PWM value for positive error rate (moving upward) and negative position error (the pitch angle value is above the reference point).

These two cases explained above are appear when the system passes the reference point with high speed and increasing position errors (positively or negatively). The other conditions in which the DTRAS system appears can easily be extracted according to the position error and error rate values.

5. EXPERIMENTAL RESULTS AND CONCLUSION

This chapter summarized the different test performed on the DTRAS and comparison is made with the corresponding simulation model results. First a set of sin and cosine trajectories were given as an inputs to the pitch and yaw controllers and comparison of the responses of the real DTRAS and its simulation model is recorded. Second, the set of step inputs given and the responses were analyzed both in simulation and real vehicle system.

In real world there are many factors that affect the system performance in a way that differ from the ideal response. So in order to operate the DTRAS close to its ideal performance the number of sources need to be added to simulate their effects on the system.

5.1. Validation of the Simulation Model

The first analysis that need to perform while investigating the system is the step response of the system. A set of step input are given as a reference input and the simulation and real system responses are recorded. The effect of cables that resist the yaw and pitch motion of the DTRAS are model by adding the necessary disturbance forces in simulation model. Also the joint friction effect is modeled in the dynamics of pitch and yaw motion.

5.2. Experimental and Simulation Response Comparision

To analyze the DTRAS dynamic responses of pitch and yaw motion, the high frequency step input is fed which have more uncertainty in corresponding output response of the system. Therefore, the step was the best choice to investigate for the system robustness and response validation level. The step input was fed to the real DTRAS setup and both the input and response were recorded. These recorded pair of information were compared to the results obtained by feeding the same step input to the validated simulation model.

5.2.1. Pitch dynamic response

Performance of pitch response for a DTRAS system with CFSF, PID and Fuzzy logic controllers are given. In Figure 5.1, the step input signal is represented for both the simulation model and the DTRAS system. It can be seen that the pitch controllers of the DTRAS system shows a similar trend in amplitude and settling with the simulation model response.
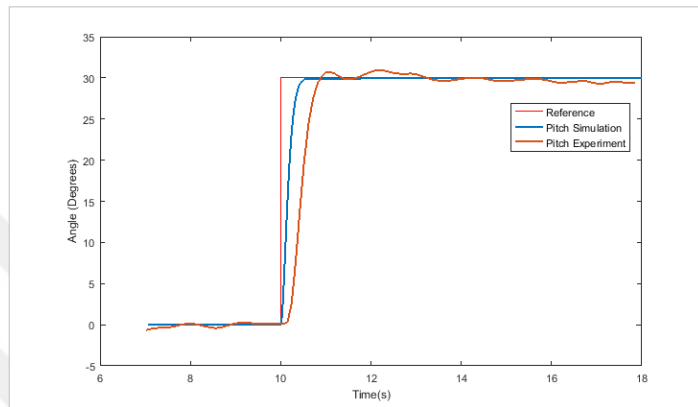
Figure 5.1. CFSF pitch controller response to step input

However, the rise time for the simulation response is less as compare to the experimental response of the DTRAS system. This is due to the fact that in the real experimentation, the controller's responses are according to the optimized gains that limits the actuating signal to the bandwidths of the motors. But in the simulation response the gains are optimized for response close to the step input without considering the maximum working bandwidth limit of the motor.

5.2.2. Yaw dynamic response

The yaw response of the DTRAS system for the CFSF controller is compared with the simulated yaw reaction as presented in Figure 5.2. Similar to the pitch response the yaw controller's responses of the DTRAS system shows similar frequency and amplitude to its simulated response.
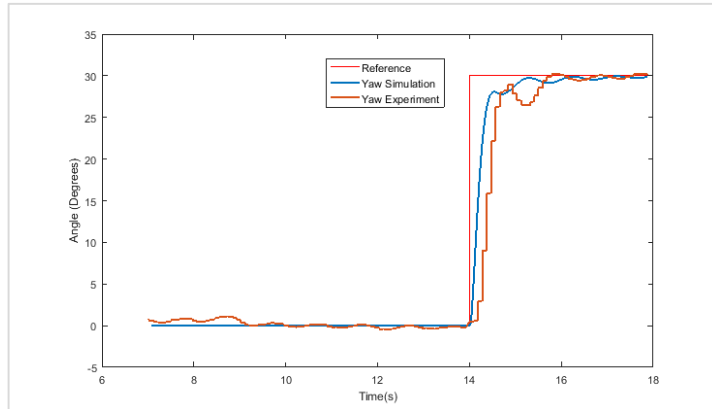
Figure 5.2. CFSF yaw controller response to step input

Nevertheless, the yaw response shows much fast tracking of the simulation response. This is because of no gravity moments that acts in case of pitch response which need to be compensated by the pitch motors by making much effort and time to reach the reference point. Besides the natural oscillations appears in the simulated response, the destabilizing much higher oscillation appears in the DTRAS system's yaw response is due to the contributed rig's moments.

5.3. Controllers Performance Comparison

For the DTRAS system three different control strategies are designed and their results are compared.
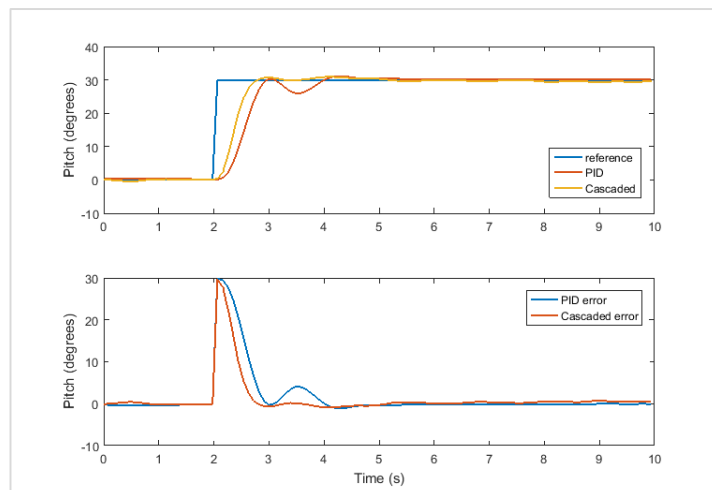
Figure 5.3. CFSF and PID controller step response and error comparison

Figure 5.3 represents the comparison between the CFSF controller and PID responses. On the other hand, the Fuzzy logic controller response is recorded separately because of the different step input magnitude value as shown in Figure 5.4. As shown in Figure 5.3, the DTRAS system shows more agile response for CFSF controller as compare to PID controller response. This agility is because of the acceleration feedback component in the most inner loop that inform the system early of any disturbance thus the controller responds quickly and get more stiff response in settling to reference point.
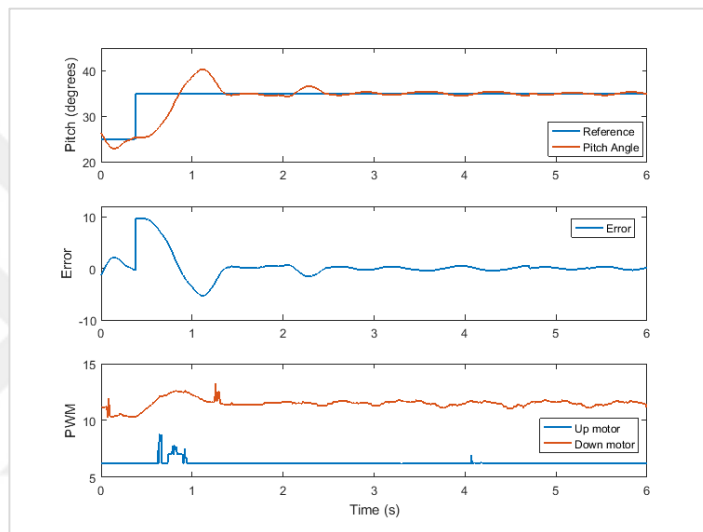
Figure 5.4. Fuzzy controller step response

The errors curve can be seen in Figure 5.3, settles early for CFSF controller in 0.8 seconds while the PID error settles to zero in 2.1 seconds.

On the other hand, in Figure 5.4, the fuzzy controller response is presented. It can be seen that the fuzzy controller response settles in 1.1 seconds with very large overshoot. The rules were designed for attaining less rising time but the results come with an overshoot of almost 50%. In future work it is decided to increase the rules resolution with optimize parameters for attaining performance.

5.4. Validation Inference

The recorded performance of the DTRAS system presented in above graphs is an evidence that the DTRAS system follows qualitatively the trends of the simulated response satisfactorily. Also controller's performance shows that CFSF controller is

the best option for the DTRAS system. The future work include modification in DTRAS system's physical configurations and implementing more advance control algorithm.

5.5. Stability Analysis of DTRAS System

In this section the stability analysis is performed by applying external disturbance to the DTRAS. The set of disturbance method are given below.

- In first stability test, the disturbance rejection capability of the controllers was investigated. This is performed by giving a gentile push with a help of stick to make movement each about pitch and yaw axis.
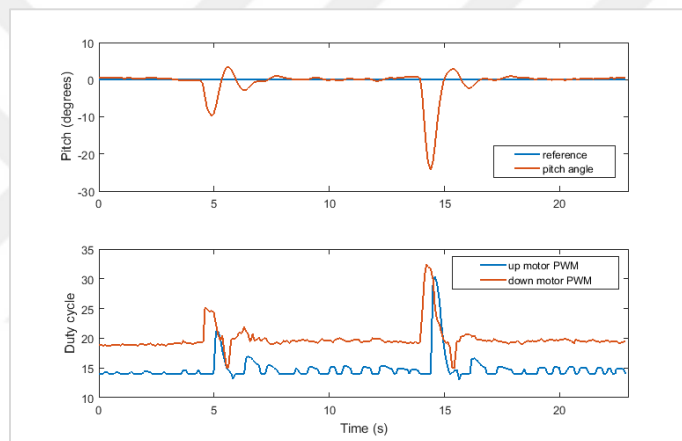
Figure 5.5. CFSF pitch controller response for a push disturbance
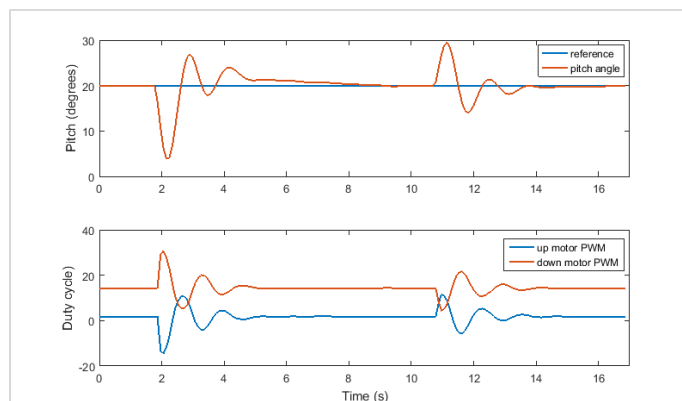
Figure 5.6. PID control response for a push disturbance

- Second, the reference tracking for each pitch and yaw controllers are performed by holding the system at specific position and release it. The response is recorded and presented in Figure 5.7.
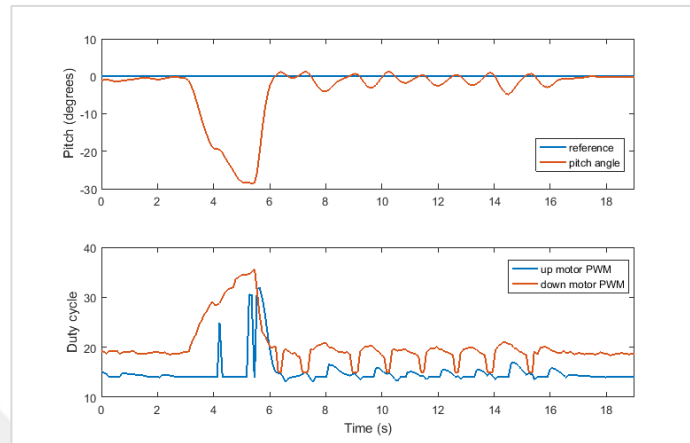
Figure 5.7. CFSF pitch controller response from hold position

For the push perturbation, the response for CFSF controller and PID controller are given in Figure 5.5 and Figure 5.6 respectively. The results show that the PID controller takes more time to reject the disturbance as compare to the CFSF controller.

5.5.1. The effect of gains on stability

The position, velocity and acceleration gains for CFSF controller are tuned using trial and error method. Figure 5.8 below shows the effect of high gains.
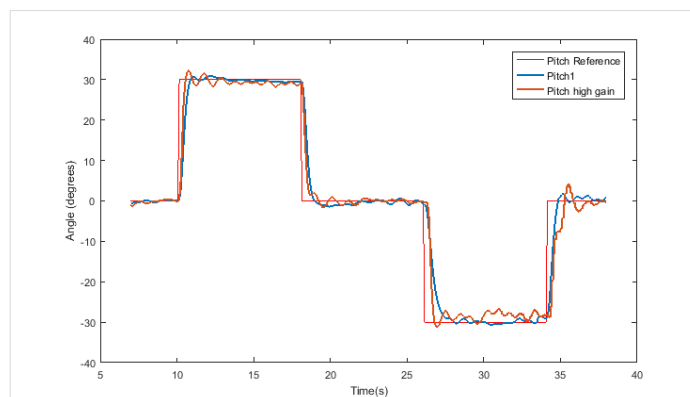
Figure 5.8. Effect of high position gain on CFSF pitch controller response

80

A very quick response with much less rising time but with more oscillation and steady state error can be seen that settles after 4 seconds. Similar behavior of the yaw dynamic can be seen in Figure 5.9. An overshoot can be seen with respect to the low gain response curve.
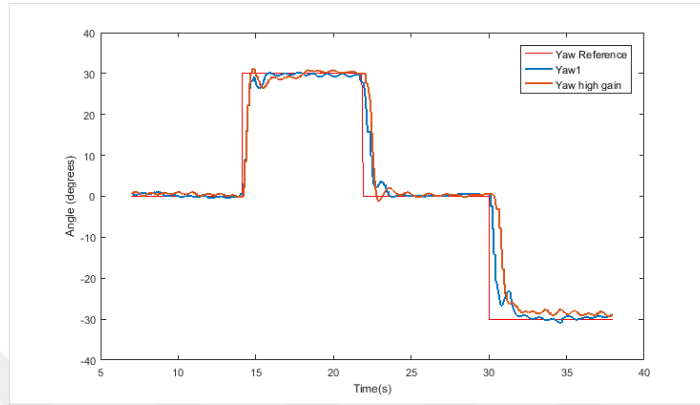
Figure 5.9. Effect of high position gain on CFSF yaw controller response

The comparison of linear and extended Kalman filters performance and its effect on the performance of the implemented controllers can be studied by investigating the stability analysis of the DTRAS system summarized in Table 5.1.

Table 5.1. Kalman Filters estimations and control stability analysis

		Pitch Controllers Stability		Yaw Controllers Stability	
		KF	EKF	KF	EKF
Maximum Overshoot M_p (%)	CFSF	14.5	12.8	1.4	1.3
	PID	8.2	7.7	13.2	12.3
	Fuzzy	50	46	19.3	20.1
Peak Time t_p (s)	CFSF	0.8	0.9	2.3	1.7
	PID	2.7	1	3.7	3.8
	Fuzzy	1.2	1.1	3.7	2.5
Settling Time t_s (s)	CFSF	1.37	1.3	2.1	1.9
	PID	2.7	2.9	5.2	5.9
	Fuzzy	3.7	3.2	4.4	3.2
Steady State error (degrees)	CFSF	3	3	2.8	3
	PID	1.7	1.8	1.8	2.1
	Fuzzy	2.6	2.1	1.7	1.7

The overshoot for all the controllers can be seen in Table 5.1, which do not vary much for linear and extended Kalman filters. The estimation results for both the filter can be seen in Figure 3.19 and Figure 3.21 shows the validation of extended Kalman filter by comparing the results with the absolute encoder reading.

In Table 5.2, the effect of measurement error of the IMU sensors on the controllers performances are investigated. The Integral Square Error (ISE) which is based on the step response of the controller's value for a particular duration of time. These results shows that, for a low value of measurement error the CFSF controller still maintain to reference point as compare to PID response. PID shows better response only at low measurement error which means measurements with white noise produce oscillation in PID response which results in higher ISE error.

Table 5.2. Controllers response errors

	ISE For Pitch Controller			ISE For Yaw Controller		
	R=0.1	R=0.3	R=0.5	R=0.1	R=0.3	R=0.5
CFSF	0.0182	0.0721	1.401	0.0522	0.0931	1.305
PID	0.0092	0.0592	3.021	0.0102	0.0481	0.0522
Fuzzy	0.0199	0.0681	1.109	0.023	0.1301	1.192

5.6. Trajectory Test

At the end of control tuning and satisfactory performance achieved, the set of trajectories were tracked. In this testing, specifically the sin, cos and sequential step trajectories were implemented. The variable of interest was recorded and the result are plotted in this section. The data recorded based on each pitch and yaw states that include the reference command signal, angular position, angular velocity and angular acceleration. To see the performance of the pitch controllers and yaw controllers, actuating signals for each motor are also recorded.
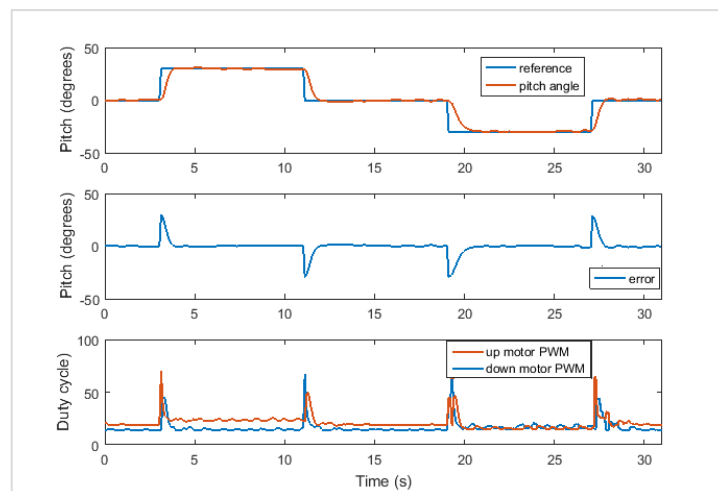
Figure 5.10. Variable step trajectory response for CFSF controller

82

As can be seen in Figure 5.10, the CFSF controller attain the set point quickly with almost no overshoot and negligible steady state error. On the other hand the PID controller response in Figure 5.11, shows an oscillation before settling to set point.
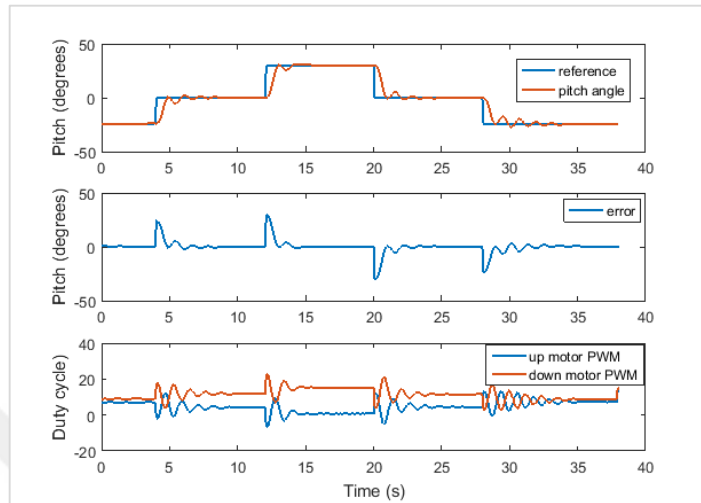
Figure 5.11. Variable step trajectory response for PID controller

Figure 5.12 presents the DTRAS response using fuzzy controller. The response can be seen have an overshoot and chattering can be seen in PWM curves for the up and down motors while switching the rules.
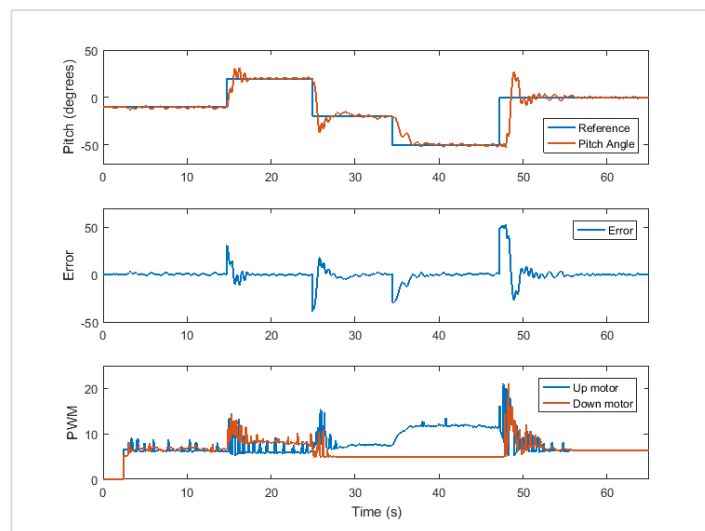
Figure 5.12. Variable step trajectory response for fuzzy controller

In the response of the DTRAS system using CFSF, PID and Fuzzy controller, the control signals for the up and down motors reduce to a minimum value. These

83

minimum value of actuating values is infact because of the minimum gravity point at which the system require less energy to attain the set point.

5.6.1. Controller effort and trajectory error

This section describes the controller's performances by comparing their efforts while tracking the variable step and sinusoidal trajectories. It can be seen in Figure 5.13, the control signal (PWM) for the up and down motors is always less in PID controller as compare to the CFSF controller. Thus the control effort by the CFSF controller is higher than the PID controller which in turn exhibit better response as can be seen in stability analysis mentioned in Table 5.1.

In DTRAS system, as mentioned in chapter 3, the pitch and yaw motions uses two motors each. Therefore, for agile response both pitch and yaw motors need high energy in form of control signal (PWM). The higher the control signal the higher the control effort and the system response will be much better, especially in term of agility.
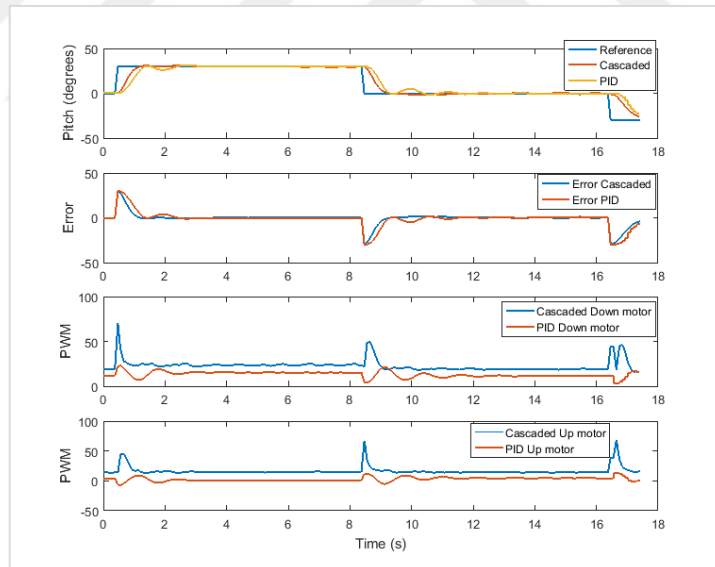
Figure 5.13. Error and actuating efforts of CFSF and PID controllers.

It can also be noted that the control effort of the down motor of the pitch rotor is always higher than the up motor during the pitch upward motion. This is due to the fact that the down motor need much energy to act against gravity moment cause by the DTRAS system weight.
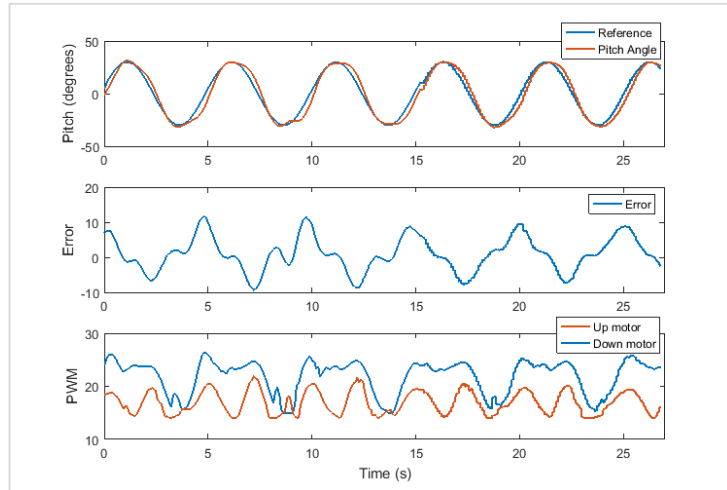
Figure 5.14. CFSF pitch controller response for sin
trajectory of $2\pi/5$ rads^{-1}

Figure 5.14 shows the sine trajectory response of the DTRAS system of $2\pi/5$ rads^{-1} frequency. Here in this case the down motor makes more effort as it has to act against gravity moment. Similar response can be seen in Figure 5.15 for yaw position motion.
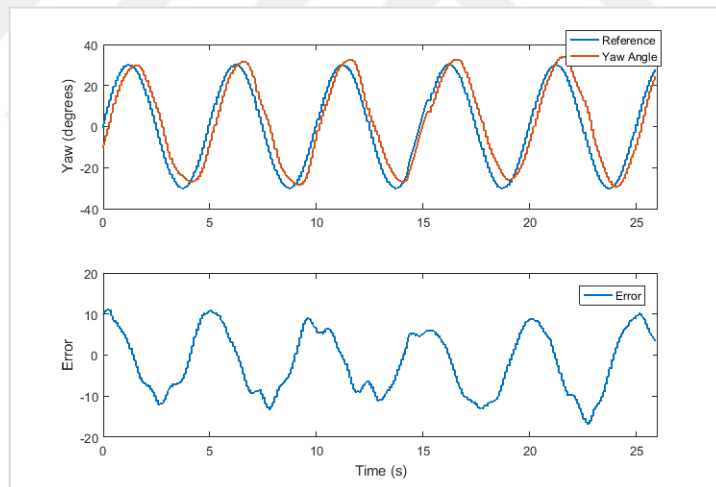
Figure 5.15. CFSF yaw controller response for sin
trajectory of $2\pi/5$ rads^{-1}

In Figure 5.16, sinusoidal trajectories of two different frequencies are feed as an input. It can be seen that the DTRAS system responses better at low frequency trajectory. The error amplitude and variation for the trajectory with frequency $2\pi/5$ rads^{-11} is higher as compare to trajectory with frequency $\pi/4$ rads^{-1}.
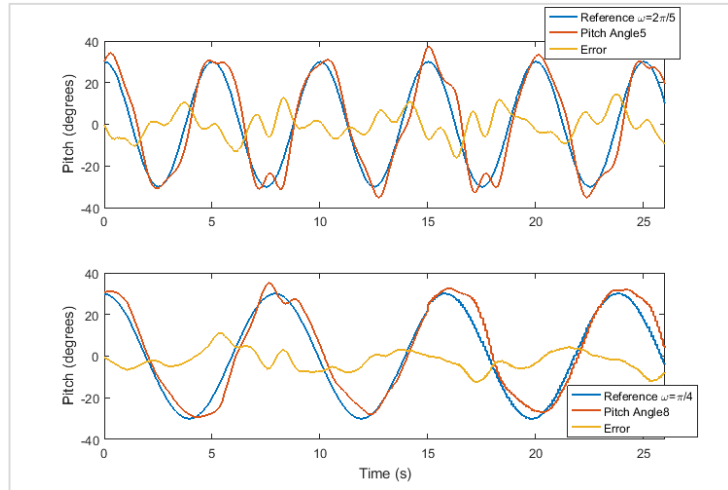
Figure 5.16. CFSF pitch response for different frequencies of sin trajectory

Figure 5.17 given below, present the 2 dimension input of variable step input to the CFSF controllers of the DTRAS system. Both the pitch and yaw reference input starts from zero degree and changes in sequence, starting from pitch input, with time interval of four seconds.
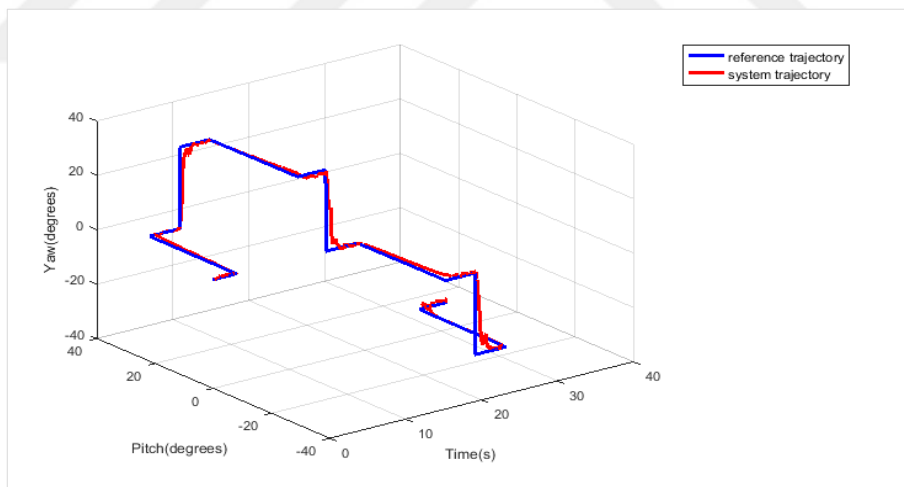
Figure 5.17. 2D step input response of pitch and yaw CFSF control

As can be seen the CFSF controllers tracks the variable step inputs with quick transient region with low positive error, as the system does not overshoot.
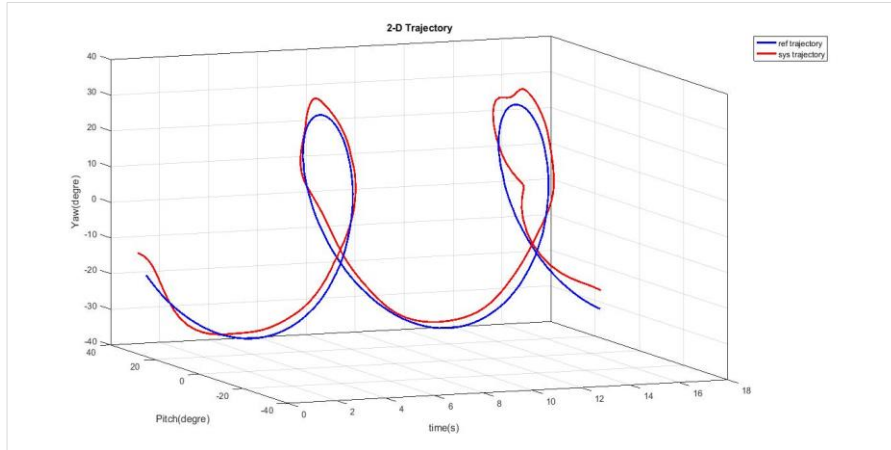
Figure 5.18. CFSF controller pitch response for

A 2-dimension sinusoidal input trajectory of sin for pitch and cos for yaw CFSF controller are fed. The response of the DTRAS system can be seen in Figure 5.18.

5.7. Conclusion

This thesis presented the control and state estimation of the novel design, 2DOF aerodynamic system. This system is the laboratory version of conventional 6DOF helicopter that is designed for investigating fast dynamic responses of pitch and yaw motion. This aerodynamics system uses two actuators for controlling each degree of freedom thus, make it an overactuated system. The mathematical modeling of the system involve physical law based on Newton laws of motion, the aerodynamic forces of the motor-propeller combination and extended Kalman filter design. Extensive identification tests of the dynamics of the actuators have been carried out. This involve the motor and propeller characterization of its parameters.

EKF is implemented for estimating the uncertain states of the proposed system from the noisy measurements from the on-board low cost IMU sensor. These estimated states are then used as states feedback information in the control algorithm for sustaining the desire attitude.

In control section three different algorithms are successfully implemented on the propose aerodynamics system. Cascaded Full-State Feedback control is a modified version of servo position control based algorithm is implemented which was a main task in control designing part of the project. For performance testing is carried out by

comparing CFSF with the PID and Fuzzy controller performances. The evidence presented shows the better performance of the CFSF control algorithm.

5.7.1. Future work

- The imprecise measurement of the physical parameters of the system mathematical model leads to the imperfect performance aberration of the aerodynamic system. Therefore, system identification technique can be performed to resolve the imperfection and mismatch.

- As the system is 2DOF, roll motion can be added to make the configuration closer in performance to the conventional helicopter system. Also the comparison can be made by testing the performance with single and double propeller in a single rotor.

- In this work, two propellers in a single rotor are used with no deep analyzation of its effect on each other. Therefore, the cross thrust effect can be further investigated to model the exact total thrust of the propulsion system unit.

- As the DTRAS system is a nonlinear system, a better nonlinear control strategy can be used to deal with the actuators and system nonlinearities for better performance.

- Selecting the suitable actuators for the particular system specifications. An actuator with high angular velocity and torque would be more performance efficient after a trade-off made in terms of its power consumption, and weight.

REFERENCES

[1]   Sikorsky I. I., Direct Lift Aircraft, 1935, U.S. Patent Number 1,994,488 Nichols, CT, United States.

[2]   Pember H., Sikorsky I. I., *Seventy-five Years of Aviation Firsts*, Stratford, Conn: Sikorsky Historical Archives, 1998.

[3]   Castillo S., Advanced Modelling of Helicopter Nonlinear Dynamics and Aerodynamics, PhD Thesis, City University London, School of Engineering and Mathematical Sciences, London, 2014.

[4]   Ho M., Helicopter in virtual space, Master Thesis, Czech Technical University, Electrotechnical Faculty, Prague, 2008.

[5]   Bodin E., Stenholm F., Modelling & Control of a 3DOF Helicopter, Bachelor Thesis, Linkoping University, Department of Management and Engineering, Lidingo, 2015.

[6]   Valavanis P. K. Vachtsevanos J. G., Dynamic Model for a Miniature Aerobatic Helicopter, Editor: Gavrilets V., *Handbook of Unmanned Aerial Vehicles*, 1st ed., Springer, Dordrecht, 279-306

[7]   Ruf M., Model Predictive Control of a Quanser 3DOF Helicopter, Master Thesis, Chalmers University, Department of Signal and System, Munich, 2014.

[8]   Gao J., Xu X., He C., A Study on the Control Methods Based on 3-DOF Helicopter Model, *Journal of Computers*, 2012, **7**(10), 2526-2533.

[9]   Schafroth, Martin D., Aerodynamics, modeling and control of an autonomous micro helicopter, Phd Thesis, ETH Zurich University, Mechanical Engineering Department, Zurich, 2010.

[10]   https://www.quanser.com/products/3-dof-helicopter/, (Visit Date: 10 January 2019).

[11]   http://www.humusoft.cz/models/ce150.htm/, (Visit Date: 10 January 2019).

[12]   Bouabdallah S., Design and control of quadrotors with application to autonomous flying, PhD thesis, Abou Bekr Belkaid University, Institute of Science and Technology, Tlemcen, 2007.

[13]   Leishman J.G., *Principles of Helicopter Aerodynamics*, 1st ed., Cambridge University Press, Cambridge, United Kingdom, 2000.

[14] Gasco P.S., Development of a Dual Axis Tilt Rotorcraft UAV: Modelling, Simulation and Control, Cranfield University, School of Engineering, Cranfield, 2012.

[15] Pounds P., Mahony R., Corke P., System identification and control of an aerobot drive system, *Information, Decision and Control*, Adelaide, Qld., Australia, 12-14 February 2007.

[16] Maia M. M., Somi P., Diez F. J., Demonstration of an Aerial and Submersible Vehicle Capable of Flight and Underwater Navigation with Seamless Air-Water Transition, *XPONENTIAL 2016 - An AUVSI Experience,* LA, United States, 2-5 May 2016.

[17] Seddon J., Newman S., *Basic Helicopter Aerodynamics*, 1st ed., American Institute of Aeronautics and Astronautics, United States, 2001.

[18] Prothin S., Moschetta S., A Vectoring Thrust Coaxial Rotor for Micro Air Vehicle: Modeling, Design and Analysis, *21st French Mechanics Congress,* Bordeaux, France, 26-30 August 2013.

[19] Paulo L. J. Drews J., Hybrid Unmanned Aerial Underwater Vehicle: Modeling and Simulation, *2014 IEEE/RSJ International Conference on Intelligent Robots and Systems*, Chicago, USA, 14-18 September 2014.

[20] Shyam, Mohan M., Mohan M., Introduction to the Kalman filter and tuning its statistics for near optimal estimates and Cramer Rao bound, *arXiv preprint arXiv:*1503.04313, 125-450, 2015.

[21] Strang G., Borre K., *Linear Algebra, Geodesy, and GPS*, 2nd ed., Wellesley Cambridge Press, Wellesley, MA, 1997.

[22] Kaplan E., Hegarty C., *Understanding GPS: Principles and Applications*, 2nd ed., Artech House, United States, 2005.

[23] Lipton A. J., Fujiyoshi H., Patil R. S., *Proceedings Fourth IEEE Workshop on Applications of Computer Vision*, NJ, USA, 19-21 October, 1998.

[24] Zarchan P., *Tactical and Strategic Missile Guidance*, 5th ed., American Institute of Aeronautics and Astronautics, USA, 2007.

[25] Roumeliotis S. I., Bekey G. A., Bayesian estimation and Kalman filtering: A unified framework for mobile robot localization, *IEEE International Conference on Robotics and Automation*, San Francisco, USA, 24-28 April 2000.

[26] Pearson J. B., Stear E. B., Kalman filter applications in airborne radar tracking*, IEEE Transactions on Aerospace and Electronic Systems*, 1974, **10**(3), 319-329.

[27] Isermann R., Process fault detection based on modeling and estimation methods, *A survey, Automatica*, 1984, **20**(4), 387-404.

[28] Ridder C., Munkelt O., Kirchner H., Adaptive background estimation and foreground detection using Kalman-filtering, *Proceedings of International Conference on Recent Advances in Mechatronics*, Istanbul, Turkey, 1995.

[29] Scharf L.L., Demeure C., *Statistical Signal Processing: Detection, Estimation, and Time Series Analysis*, 2nd ed., Addison Wesley, United States, 1991.

[30] Gannot S., Burshtein D., Weinstein E., Iterative and sequential Kalman filter-based speech enhancement algorithms, *IEEE Transaction Speech and Audio Processing*, 1998, **6**(4), 373-385.

[31] Erturk S., Real-time digital image stabilization using Kalman filters, *Real-Time Imaging*, 2002, **8**(4), 317-328.

[32] Kiencke U., Nielsen L., *Automotive control systems: For engine, driveline, and vehicle*, 2nd ed., Springer, United States, 2005.

[33] Faragher R., Understanding the Basis of the Kalman Filter Via a Simple and Intuitive Derivation", *IEEE signal processing magazine,* 2012, **29**(5), 128-132.

[34] Brown R.G., Hwang P.Y.C., *Introduction to Random Signals and Applied Kalman Filtering,* 2nd ed., John Wiley & Sons, Inc., United States, 1998.

[35] Grewal M.S., Andrews A.P., *Kalman Filtering: Theory and Practice Using MATLAB*, 4th ed., John Wiley & Sons, Inc., United States, 1992.

[36] Yongliang W., Tianmiao W., Attitude Estimation for Small Helicopter Using Extended Kalman Filter, *2008 IEEE Conference on Robotics, Automation and Mechatronics*, Beijing China, 21-24 September 2008.

[37] Ascorti L., An application of the extended kalman filter to the attitude control of a quadrotor, Master Thesis, Politecnico Di Milano, Computer Engineering department, Milano, 2013.

[38] Christopher A.M., An application of Extended Kalman filtering to a model-based, short-range navigator for an AUV, Master Thesis, Defense Technical Information Center, Naval Postgraduate School, Monterey, 1991.

[39] Pettersson M., Extended Kalman Filter for Robust UAV Attitude Estimation, Master Thesis, Linköping University, Faculty of Science and Engineering, Valla, 2015.

[40] Kalman R.E., Bucy R.S., New results in linear filtering and prediction theory, *Journal of basic Engineering*, 1961, **83**(3), 95-108.

[41] Kalman R.E., A new approach to linear filtering and prediction problems, *Journal of basic Engineering*, 1960, **82**(1), 35-45.

[42] Harkegard O., Backstepping and Control Allocation with Applications to Flight Control, PhD thesis, Linköping University, Faculty of Science and Engineering, Valla, 2003.

[43] Salas O., Castañeda H., Morales J.D.L., Observer-Based Attitude Control for a Two-rotor Aerodynamical System, *2013 Physcon*, San Luis Potosoi, Mexico, 26-29 August 2013.

[44] Butt S., Prabel, R., Aschemann H., Multi-Variable Flatness-Based Control of a Helicopter with Two Degrees of Freedom, *2014 International Conference on Control, Decision and Information Technologies*, Metz France, 3-5 November 2014.

[45] https://www.emaxmodel.com/cf2822.html (Visit Date: 4th March 2019).

[46] https://www.getfpv.com/tiger-motor-f40-pro-2400kv-fpv-series-motor-1pc.html (Visit Date: 4th March 2019).

[47] Al-Rihani Y., Development of a Dual Axis Tilt Rotorcraft UAV: Design, Prototyping and Control, Master Thesis, Cranfield University, School of Engineering, Bedfordshire, 2012.

[48] https://www.miniquadtestbench.com/assets/components/motordata/motorinfo.php?uid=203 (Visit Date: 4th March 2019).

[49] https://www.youtube.com/watch?v=K-opRoroEAg (Visit Date: 4th March 2019).

[50] URL-7https://www.banggood.com/T-Motor-F30A-FPV-30A-2-4S-ESC-BLHeli_S-Dshot-Oneshot125-Oneshot42-Multishot-For-FPV-Racing-p-1110027.html? cur warehouse=CN (Visit Date: 4th March 2019).

[51] URL-8 http://www.chrobotics.com/shop/um7-lt-orientation-sensor (Visit Date: 4th March 2019).

[52] Dunn F., Parberry I., *3D Math Primer for Graphics and Game Development Wordware Game Math Library*, 2nd ed., CRC press, London, 2011.

[53] Leishman J.G., *Principles of Helicopter Aerodynamics. Cambridge Aerospace Series*, 1st ed., Cambridge University Press, London, 2006.

[54] Martin S.D., Aerodynamics, Modeling and Control of an Autonomous Micro Helicopter, Phd Thesis, Eth Zürich, deparment, city, Swiss Federal Institute of Technology Zurich, Lützelflüh, 2010.

[55] Ling G., Persson J., Propulsion Unit of a 3DOF Helicopter, Bachelor Thesis, Linköping University, Faculty of Science and Engineering, Valla, 2015.

[56] Abyarjoo F., Barreto A., Cofino J., Ortega F., Implementing a Sensor Fusion Algorithm for 3D Orientation Detection with Inertial/Magnetic Sensors, Editors: Sobh, T., Elleithy, K., Innovation and Advances in Computing, Informatics, Systems Sciences, Networking and Engineering, 1st ed., Springer Cham, London, 305-310, 2015.

[57] Khalesi M.H., Salarieh H., Foumani M.S., Dynamic Modeling, Control System Design and MIL-HIL Test of an Unmanned Rotorcraft Using Novel Low-Cost Flight Control System, *Iranian Journal of Science and Technology, Transection of Mechanical Engineering*, 2019, **4**(16), 1-20.

[58] Thrun S., Burgard W., Fox D., *Probabilistic Robotics*, 1st ed., Mit Press, United States, 2005.

[59] Arimoto S., Miyazaki F., Stability and robustness of PID feedback control for robot manipulators of sensory capability, *Robotics research: First international symposium,* Cambridge, 1984.

[60] Sciavicco L., Siciliano B., *Modelling and control of robot manipulators*, 2nd ed., Springer, London, 2000.

[61] Azeem M.F., *Fuzzy Inference System: Theory and Applications,* 1st ed., IntechOpen, London, 2012.

[62] Aguilar R.M., Muñoz V., and Callero Y., *Control Application Using Fuzzy Logic: Design of a Fuzzy Temperature Controller*, 1st ed., IntechOpen, London, 2005.

APPENDICES

APPENDIX-A

Absolute Maximum Ratings			
Parameter	HEDS-55XX/56XX	HEDM-550X/560X	HEDM-5540
Storage Temperature, T_S	-40°C to 100°C	-40°C to +70°C	-40°C to 85°C
Operating Temperature, T_A	-40°C to 100°C	-40°C to +70°C	-40°C to 85°C
Supply Voltage, V_{CC}	-0.5 V to 7 V	-0.5 V to 7 V	-0.5 V to 7 V
Output Voltage, V_O	-0.5 V to VCC	-0.5 V to VCC	-0.5 V to VCC
Output Current per Channel, I_{OUT}	-1.0 mA to 5 mA	-1.0 mA to 5 mA	-1.0 mA to 5 mA
Vibration	20 g, 5 to 1000 Hz	20 g, 5 to 1000 Hz	20 g, 5 to 1000 Hz
Shaft Axial Play	± 0.25 mm (± 0.010 in.)	± 0.175 mm (± 0.007 in.)	± 0.175 mm (± 0.007 in.)
Shaft Eccentricity Plus Radial Play	0.1 mm (0.004 in.) TIR	0.04 mm (0.0015 in.) TIR	0.04 mm (0.0015 in.) TIR
Velocity	30,000 RPM	30,000 RPM	30,000 RPM
Acceleration	250,000 rad/sec^2	250,000 rad/sec^2	250,000 rad/sec^2

Figure A.1. Electrical Rating for Pitch Encoder HEDS 5500

Figure A.2. Dimensions of Pitch Encoder HEDS 5500

	HE□□B -□-□-□-N-□	HE□□B -□-□-□-O-□	HE□□B -□-□-□-T-□	HE□□B -□-□-□-L-□
Mode				
Output type	NPN Voltage output	NPN Open collector output	Totem Pole output	Line Drive output
Output signal	A, B, Z phase			A,B,Z,$\overline{A}$,$\overline{B}$,$\overline{Z}$ phase
Phase difference on Output	Phase difference between A, B phase : T/4 ± T/8(Cycle of A phase = T)			
Max Response Frequency	300 kHz			
Power voltage	5 – 12 V DC / 12 – 24 V DC ± 5 %			5/12/24 V DC ±5 %
Current Consumption	60 mA max. (No-load)			
Connection method	Cable extended type			
Control output	Load voltage : 30 V max. Load Current : 30 mA max. Residual Voltage : 0.4 V max.		For Low Load Current : 30 mA max. Remaining Voltage : 0.4 V max. For High Load Current : 10 mA max. Remaining Voltage : Power Voltage 2.5 V min.	For Low Load Current : 20 mA max. Remaining Voltage : 0.4 V max. For High Load Current : 20 mA max. Remaining Voltage : 2.5 V min.
Response Time	1μs max. (Cable length 1.5 m / sink= 30 mA)		1μs max. (Cable length 1.5 m / sink=10 mA)	1μs max.(Cable length 1.5 m / sink = 30 mA)

(Electrical Specification)

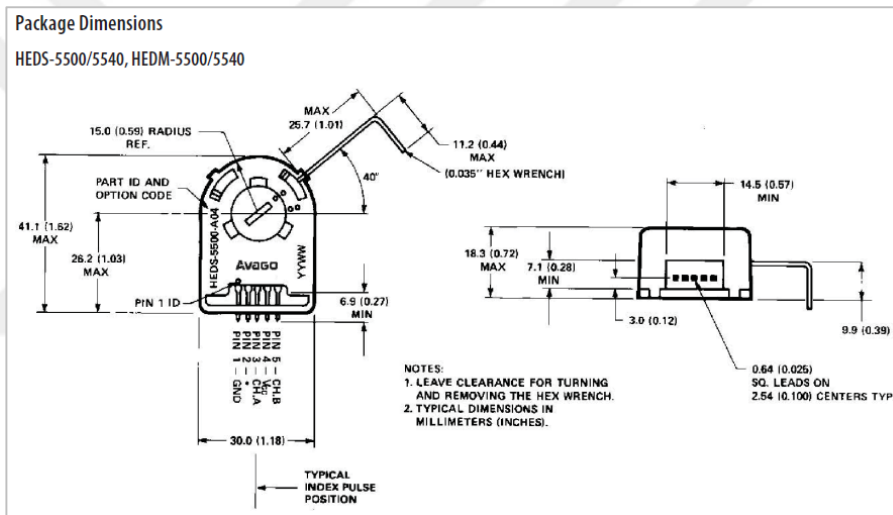Figure A.3. Electrical Ratings of Yaw Encoder HE40B

Figure A.4. Dimensions of Yaw Encoder HE40B

APPENDIX-B

Features
- Adopt high-performance DSP and FPGA technology
- Each card can control 8 servo/step motors
- Programmable sampling rate. The minimum interpolation period of four axes is 200µs. The minimum control period of single-axis point-to-point motion is 25µs.
- Modes of motion: point-to-point motion, linear interpolation, circular interpolation, velocity control, interface to manual pulse generator, and electronic gearing
- Programmable trapezoid curve planning and S-curve planning and update parameters on-the-fly
- All the position and parameters registers are of 32 bits
- Hardware capture of home switch and index signal of encoder
- Set following-error limit, acceleration limit and output limit, to ensure safe and

Figure B.1. Common Features of GoogolTech

Specification

Dedicated Digital Input/Output
- Dedicated opto-isolated inputs: 2 for limit switches, 1 for home switch and 1 for driver alarm signal input for each axis
- Dedicated opto-isolated outputs: 1 for driver enable signal and 1 for reset driver alarm signal for each axis
- 3 dedicated inputs for protection: abrupt stop, door stop and logical stop

Software Characteristics
- User-defined coordinate system for ease of programming
- 4-D coordinated motion
- Continuous interpolation
- Motion command buffer for increasing communication efficiency
- Programmable event interrupt: external input interrupt, event interrupt and timer interrupt
- EEPROM for updating Firmware and system parameters
- Windows98/2000/NT/XP drivers and DLL, C and C++ function library

Channels of Input/Output
- 8 channels of output, ±10V analog voltage with 16-bit resolution control signal
- 8 channels of quadrature incremental encoder input for the feedback of each axis
- 4 channels of quadrature incremental encoder input for the auxiliary encoder input
- Encoder sampling rate up to 8MHz
- 2 channel of D/A output
- 8 channels of encoder input with 8-bit resolution and sampling rate up to 8MHz

Output Range
- Position: 32-bit (2.15 billions of pulses)
- Velocity: Up to 8 millions of pulses/second for servo motor
- Acceleration: Up to 16 millions of pulses/second

Figure B.2. GoogolTech dspace Spesifications

PUBLICATIONS

[1] **Nasir F**., Fatuhi M. J., Bingul Z., Linear and Extended Kalman Filter Estimation of Pitch and Yaw Angles for 2 DOF Double Dual Twin Rotor Aero-dynamical System, *2018 6th International Conference on Control Engineering & Information Technology (CEIT),* Istanbul, Turkey, 25-27 October 2018.

[2] Khan M.T., Izhar, **Nasir F**., Qadir M.U., Multi-Robot Cooperation Framework Based on Artificial Immune System, *Mechatronic Systems and Control,* 2015, **43**(3), 159-167.

[3] Khan M.T., Qadir, M.U., Abid A., **Nasir F**., Silva C.W., Robot Fault Detection Using an Artificial Immune System (AIS), *Mechatronic Systems and Control,* 2015, **43**(2), 107-117.

[4] Khan M.T., Izhar, **Nasir F**., Qadir M.U., Silva C.W., Artificial Immune System Based Framework for Multi-Robot Cooperation, *The 9th International Conference on Computer Science & Education (ICCSE 2014),* Vancouver, Canada, 22-24 August 2014.

[5] Khan M.T., Qadir M.U., **Nasir F**., Silva C.W., A Framework for a Fault Tolerant Multi-Robot System, *The 10th International Conference on Computer Science & Education (ICCSE 2015),* Cambridge University, UK, 22-24 July 2015.

RESUME

Fazal E Nasir was born in 1990 in Peshawar, Pakistan. After finishing his high school from Army Public School and Degree College Peshawar, he started Mechatronics Engineering from University of Engineering and Technology (UET) Peshawar, Pakistan and graduated in 2013. Amid his BS studies in Mechatronics he joined as apprentice in Robotics & Automation Laboratory and Control System & Microcontroller Laboratory in Institute of Mechatronics Engineering, UET Peshawar, where he worked on various commercial and academic projects. He has served in Robotics Club UET Peshawar 2012-13 as Technical Head to supervise and screen specialized issues in robotics. Later on he got a chance to work in heading air ship manufacturing and assembling organization, Pakistan Aeronautical Complex (PAC) Kamra, in maintenance section. In the year 2015, He secured Turkish government scholarship for studying his master degree in mechatronics engineering from Kocaeli University, Turkey.